RESEARCH LETTER

Integrative metagenomics and metabolomics reveal age-associated gut microbiota and metabolite alterations in a hamster model of COVID-19

Patrícia Brito Rodrigues[a*], Vinícius de Rezende Rodovalho [b*$], Valentin Sencio[a], Nicolas Benech[c,d,e], Marybeth Creskey[f], Fabiola Silva Angulo[a], Lou Delval[a], Cyril Robil[a], Philippe Gosset[a], Arnaud Machelart[a], Joel Haas[g], Amandine Descat[h], Jean François Goosens[h], Delphine Beury[i], Florence Maurier[i], David Hot[i], Isabelle Wolowczuk[a], Harry Sokol [c,d,j], Xu Zhang[f,k], Marco Aurélio Ramirez Vinolo[b*], and François Trottein [a*]

aU1019 - UMR 9017 - CIIL - Center for Infection and Immunity of Lille, University of Lille, CNRS, Inserm, CHU Lille, Institut Pasteur de Lille, Lille, France; bLaboratory of Immunoinflammation, Institute of Biology, University of Campinas (UNICAMP), Campinas, Brazil; cGastroenterology Department, Sorbonne Université, Inserm, Centre de Recherche Saint-Antoine, CRSA, AP-HP, Saint Antoine Hospital, Paris, France; dParis Center for Microbiome Medicine, Fédération Hospitalo-Universitaire, Paris, France; eHospices Civils de Lyon, Lyon GEM Microbiota Study Group, Lyon, France; fRegulatory Research Division, Biologic and Radiopharmaceutical Drugs Directorate, Health Products and Food Branch, Health Canada, University of Ottawa, Ottawa, Canada; gU1011-EGID, University of Lille, Inserm, CHU Lille, Institut Pasteur de Lille, Lille, France; hEA 7365 - GRITA - Groupe de Recherche sur les formes Injectables et les Technologies Associées, University of Lille, CHU Lille, Lille, France; iUS 41 - UAR 2014 - PLBS, University of Lille, CNRS, Inserm, CHU Lille, Institut Pasteur de Lille, Lille, France; jINRAE, AgroParisTech, Micalis Institute, Université Paris-Saclay, Jouy-en-Josas, France; kSchool of Pharmaceutical Sciences, Faculty of Medicine, University of Ottawa, Ottawa, Canada

ABSTRACT

Aging is a key contributor of morbidity and mortality during acute viral pneumonia. The potential role of age-associated dysbiosis on disease outcomes is still elusive. In the current study, we used high-resolution shotgun metagenomics and targeted metabolomics to characterize SARS-CoV-2-associated changes in the gut microbiota from young (2-month-old) and aged (22-month-old) hamsters, a valuable model of COVID-19. We show that age-related dysfunctions in the gut microbiota are linked to disease severity and long-term sequelae in older hamsters. Our data also reveal age-specific changes in the composition and metabolic activity of the gut microbiota during both the acute phase (day 7 post-infection, D7) and the recovery phase (D22) of infection. Aged hamsters exhibited the most notable shifts in gut microbiota composition and plasma metabolic profiles. Through an integrative analysis of metagenomics, metabolomics, and clinical data, we identified significant associations between bacterial taxa, metabolites and disease markers in the aged group. On D7 (high viral load and lung epithelial damage) and D22 (body weight loss and fibrosis), numerous amino acids, amino acid-related molecules, and indole derivatives were found to correlate with disease markers. In particular, a persistent decrease in phenylalanine, tryptophan, glutamic acid, and indoleacetic acid in aged animals positively correlated with poor recovery of body weight and/or lung fibrosis by D22. In younger hamsters, several bacterial taxa (*Eubacterium*, *Oscillospiraceae*, *Lawsonibacter*) and plasma metabolites (carnosine and cis-aconitic acid) were associated with mild disease outcomes. These findings support the need for age-specific microbiome-targeting strategies to more effectively manage acute viral pneumonia and long-term disease outcomes.

Introduction

Older adults (over ~65 years) are particularly susceptible to respiratory viral infections, including those caused by influenza A viruses and severe acute respiratory syndrome coronavirus 2 (SARS-CoV-2), the etiologic agent of coronavirus disease-19 (COVID-19).[1-3] This greater susceptibility to viral infections in the elderly is related to declines in pulmonary function and immune response, as well as altered recovery, prolonging the duration of sequelae.[4-6] It is well established that the gut microbiota plays a key role in the lung's defense against respiratory viruses.[7,8] Recent clinical studies have also shown that alterations of the gut

microbiota's functionality during influenza and COVID-19 correlate with disease severity and/or long-term sequelae.[9–24] However, human studies investigating the effects of viral pneumonia on the preexisting altered microbiota in older adults are sparse. We herein investigated for the first time the effects of a respiratory virus (SARS-CoV-2) on the gut microbiota's functionality in a preclinical model of advanced aging. To this end, the Syrian golden hamster, a valuable model of COVID-19 research,[25,26] was used.

Aging associates with perturbations in gut microbiota composition and functionality.[27,28] In both humans and mice, aging is associated with a decline in microbial diversity and richness, including a notable decrease in beneficial bacteria like the short-chain fatty acid (SCFA)-producing Lachnospiraceae, Ruminococcaceae, and Bifidobacteriaceae family members.[28–33] Conversely, there is an increased relative abundance of the Pseudomonadota phylum (formerly termed as Proteobacteria), which may drive inflammaging.[28] Importantly, aging is associated with defects in multiple crucial metabolic functions of the gut microbiome. Several metabolic pathways are affected including those involved in the production of SCFAs, tryptophan metabolites (indole), and secondary biliary acid.[28–33] Interestingly, some products of these metabolic pathways play a role in the control of respiratory viral infections in both mice and humans.[34–39] Despite these clear alterations of the aged gut microbiota, few studies have explored the link between age-related dysbiosis and susceptibility (and severity) to viral respiratory infections. Fuentes and colleagues reported that the abundances of specific bacteria, including butyrate-producers and members of Gammaproteobacteria family, could serve as potential biomarkers for susceptibility to influenza infection in aged individuals.[15] In a clinical study on COVID-19, MacCann and colleagues showed that the proliferation of opportunistic pathogens, such as *Clostridium hathewayi*, *Enterococcus faecium*, *Coprobacillus*, *Eggerthella*, *Actinomyces spp.*, *Ruminococcus gnavus*, *Ruminococcus torques*, and *Bacteroides dorei*, correlated with dysregulated inflammatory response and disease severity in aged individuals.[20] SARS-CoV-2 has been shown to alter the gut microbiota composition in hamsters,[26,40] although the impact of advanced age remains unknown. In the current study, we investigated the relationship between age, gut microbiota, and SARS-CoV-2 infection, focusing on: (1) the association between age-related changes in gut microbiota and COVID-19 susceptibility and outcomes, and (2) the differential impact of SARS-CoV-2 infection on the gut microbiota of young adults versus aged individuals, and its potential influence on disease parameters. To investigate this, two-time points were studied: one corresponding to the peak of disease severity and another related to disease resolution. We combined shotgun metagenomics, targeted metabolomics, and measurements of COVID-19 severity. This multi-omics approach allowed us to identify a specific signature potentially linked to gut microbiota that is associated with disease outcomes in advanced aged individuals.

Results

Aged hamsters exhibit alterations of gut microbiota composition and functionality at steady state

The aging process affects the composition and functional activity of the gut microbiota in both humans and rodents[41–43] but its impact on hamster's gut microbiota has not been studied until now. To address this knowledge gap, cecal samples were collected from young (2-month-old) and aged (22-month-old) hamsters and processed for metagenomics analysis ($n = 3$ and $n = 6$, respectively). Shotgun metagenomic sequencing showed no significant differences in bacterial alpha diversity between the two age groups (Shannon index, genus level) (Supplementary Figure S1a). However, beta diversity analysis (species level), using an Aitchison distance-based principal coordinate analysis (PCoA), revealed significant differences in the bacterial communities between young and aged hamsters ($p = 0.016$ and $R2 = 0.33$, permutational multivariate analysis of variance, PERMANOVA) (Figure 1(a)). Consistent with previous studies using 16S rRNA gene sequencing,[26,40,44] shotgun analysis revealed that Bacillota (formerly Firmicutes) and Bacteroidota (Bacteroidetes) dominated the gut microbiota in hamsters. There was no significant change in their abundance with aging (73.3/69.6% and 24.5/27.5% in young/aged hamsters, respectively)
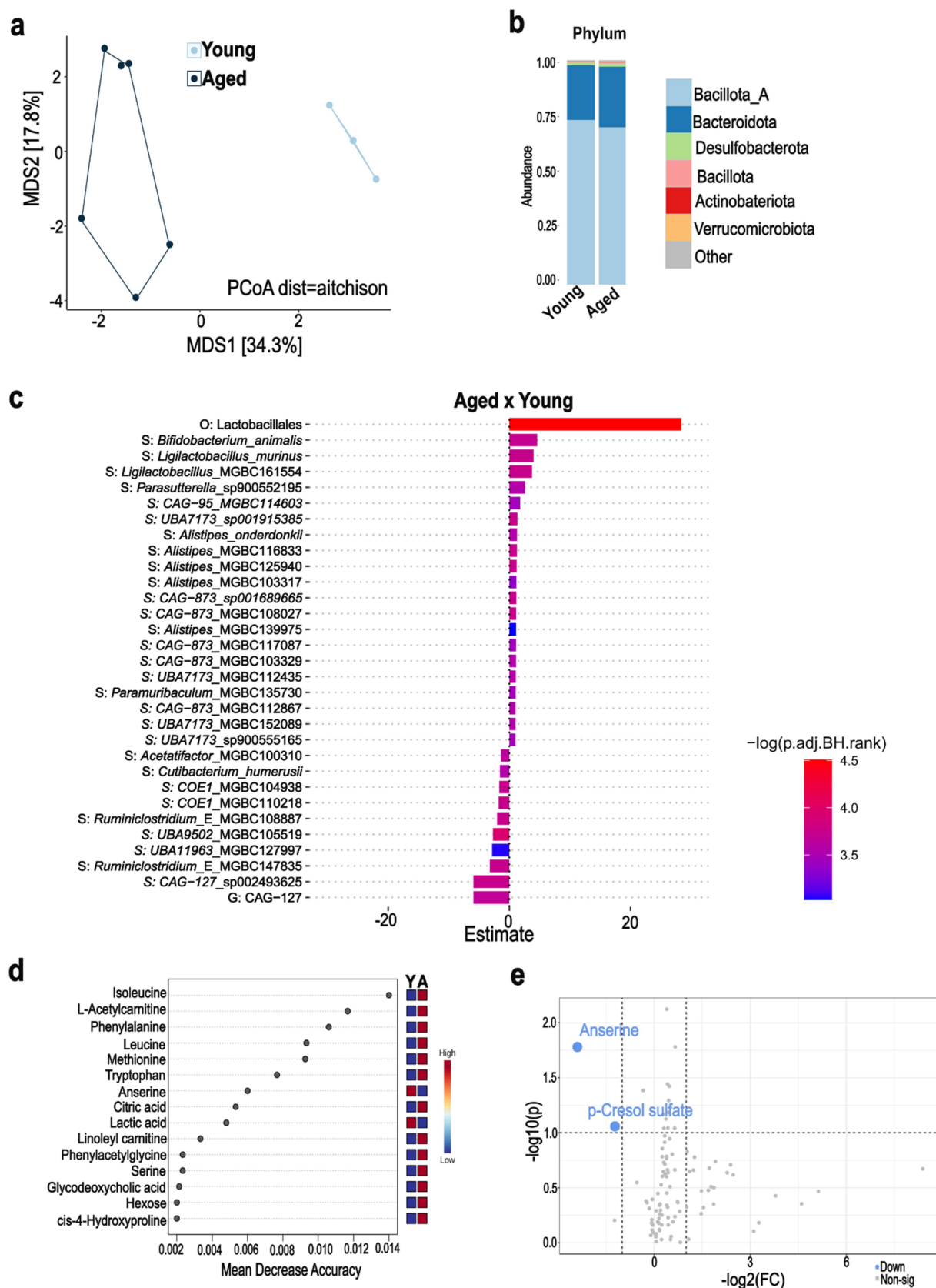
Figure 1. Shotgun metagenomics and plasma metabolome analysis from young and aged hamsters (steady state). a, PCoA plot (species) representing microbial β-diversity based on Aitchison distance metric (PERMANOVA, $p = 0.013$) b, gut microbiota composition at the phylum level. c, differential abundance of taxa analyzed with Maaslin2 (adjusted P-value < 0.05). d, ranking of the 15 most important metabolites from the 104 total plasma metabolites identified by random forest, based on mean decrease accuracy. Colored boxes indicate relative concentrations of metabolites in each group (young: Y, aged: A). e, volcano plot of plasma metabolite differential abundance between young and aged hamsters. The y-axis represents the − log10 adjusted p value (dashed line at $a = 0.05$), and the x-axis represents the log2 FC (dashed line at two fold change) ($n = 3–6$/group).

(Figure 1(b)). At the genus level, *UBA9475*, *Oscillibacter*, *Alistipes*, *Acetatifactor*, *Amulumruptor*, and *Bacteroides* were the most abundant taxa, with no significant differences between the young and aged groups (Supplementary Figure S1b). A linear regression model revealed significant differences in the abundance of specific bacterial species between young and aged hamsters (Figure 1(c) and Supplementary Table S1). The main change at the order level was an increase in Lactobacillales abundance in aged hamsters. Compared to young animals, aged hamsters had higher relative abundances of *Bifidobacterium_animalis*, *Ligilactobacillus_murinus*, *Ligilactobacillus*_MGBC161554, *Parasutterella*_sp900552195, and *Alistipes sp.* (Figure 1(c)). In the young group, enriched species included several *Ruminiclostridium* strains and members of the Lachnospiraceae family (*e.g.*, species *CAG-127_sp002493625*).

Given the established link between gut microbiota and host metabolism,[43,45] we then assessed the impact of aging on plasma metabolites. Targeted quantitative metabolomic analysis was performed on plasma samples using liquid chromatography coupled with tandem mass spectrometry (LC-MS/MS). Hierarchical clustering analysis indicated differences in the metabolites concentrations between young and aged hamsters (Supplementary Figure S1c). Multivariate analysis with random forest[44] identified several metabolites that discriminate between young and aged hamsters, including amino acids and their derivatives (isoleucine, phenylalanine, leucine, methionine, tryptophan, anserine, serine, and phenylacetylglycine), carnitines (l-acetylcarnitine and linoleyl carnitine), secondary bile acids (glycodeoxycholic acid) and components involved in energy metabolism (citric acid, lactic acid, and hexose) (Figure 1(d)). We also employed univariate statistical analysis to investigate differences in metabolites between aged and young hamsters. Compared to their young counterparts, aged hamsters showed a significant reduction in p-cresol sulfate, a tyrosine-derived metabolite linked to gut microbiota metabolism,[46] and anserine, a bioactive dipeptide acting through the gut microbiota[47] (fold change threshold = 2.0, $p < 0.05$, Figure 1(e)). We conclude that at steady state (no infection), aged hamsters display notable changes in the composition and metabolic function of the gut microbiota.
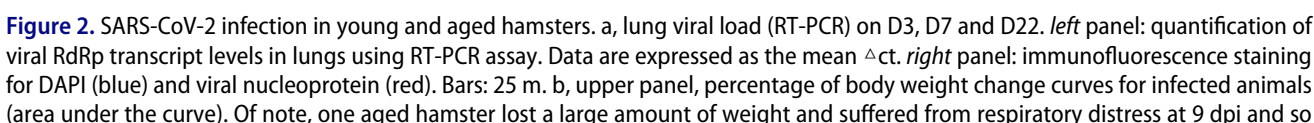
Aged hamsters have high pulmonary viral load, display a specific lung transcriptomic signature and develop post-acute sequelae

Age-related gut dysbiosis increases susceptibility to various diseases[28,48–51] but its impact on respiratory infections remains largely unexplored. We therefore compared the outcomes of a SARS-CoV-2 infection in young and aged hamsters using a prototypic ancestral strain of the virus. Hamsters from each group were sacrificed on day 3 post-infection (D3), the peak of lung viral load ($n = 6$); on D7, the peak of the acute phase response ($n = 6$); and on D22, the resolving phase of infection ($n = 6$ for young animals and $n = 3$ for aged animals) (Supplementary Figure S2a).[26,52] Quantitative RT-PCR revealed that aged hamsters presented a significantly higher lung viral load than young hamsters on both D3 and D7 (Figure 2(a), *left* panel). Immunofluorescence staining confirmed the high viral load in aged animals (Figure 2(a), *right* panel and not shown). By D22, no viral transcripts were detected, indicating complete viral clearance.

Compared to young hamsters, aged animals did not experience a greater body weight loss until D6 (Figure 2(b)). However, while young hamsters began to recover from D7 onwards, aged animals continued to lose body weight until D8 and did not regain their initial body weight on D22 (Figure 2(b) and Supplementary Figure S2b).

Histopathology analysis (hematoxylin & eosin staining) showed that lung damage in terms of inflammation, hemorrhage, type 2 hyperplasia, and edema was similar in young and aged hosts on D7 (Figure 2(c)). Regarding these criteria, lung damage was strongly reduced by D22.

Compared to the young group, pulmonary gene expression of C-X-C motif chemokine ligand 10 (*Cxcl10*) and interferon-stimulated gene 15 (*Isg15*) (representative of ISGs), but not chemokine ligand 2 (*Ccl2*) and interleukin-6 (*Il6*) (representative of inflammation), was higher in the aged group on D7 (Supplementary Figure S2c). Gene expression of the tight junction proteins zonula occludens 1 (*Zo1*) and occludin (*Ocln*) was reduced in the

Figure 2. SARS-CoV-2 infection in young and aged hamsters. a, lung viral load (RT-PCR) on D3, D7 and D22. *left* panel: quantification of viral RdRp transcript levels in lungs using RT-PCR assay. Data are expressed as the mean △ct. *right* panel: immunofluorescence staining for DAPI (blue) and viral nucleoprotein (red). Bars: 25 m. b, upper panel, percentage of body weight change curves for infected animals (area under the curve). Of note, one aged hamster lost a large amount of weight and suffered from respiratory distress at 9 dpi and so

aged group, indicating elevated alteration of the epithelial barrier (Supplementary Figure S2d).

To further explore the effects of aging on pulmonary gene expression, bulk RNA sequencing (RNAseq) was performed on lung tissue at D7 (n = 3–4/group). This analysis revealed distinct differences in gene expression between young and aged hamsters, as illustrated by Venn diagrams (Supplementary Figure S2e) and volcano plots (Figure 2d and Supplementary Table S2). A substantial portion of the differentially expressed genes (DEGs) was shared between young and aged hamsters (40–45%, gene ontology enrichment analysis in Supplementary Figure S2f). Young and aged hamsters also had exclusive DEGs, with most being upregulated in aged hamsters (1,178/1,501) and downregulated in young hamsters (1,660/1,937). Pathways induced in infected aged hamsters included those related to protein synthesis and degradation (*e.g.*, "proteasome" and "protein processing in endoplasmic reticulum") and immune activation ("Epstein-Barr Virus infection", "Immunity", "Lysosome" and "NF-kappa B signaling pathway"), indicating increased protein turnover and intense immune activation (Figure 2(e), *upper* panel). Genes exclusively downregulated in young hamsters were associated with transcription regulation and metabolism (e.g., "Propanoate metabolism", "Valine, leucine, and isoleucine degradation", "Lipid metabolism" pathways), as well as "Platelet activation" (Figure 2(e), *lower* panel).

Clinical and experimental evidence suggests that severe respiratory viral infections can lead to persistent lung pathology, remodeling and pulmonary dysfunction.[53–55] The kinetics of lung damage after acute SARS-CoV-2 infection was then assessed through Sirius Red staining of lung sections. Aged hamsters had a significantly higher percentage of Sirius Red staining (a marker of fibrosis) on D22 compared to young animals (Figure 2(f)). Accordingly, transcript expression levels of markers associated with pulmonary fibrosis such as collagen 1 alpha 1 (*Col11*), *Col3a1*, extracellular matrix protein 1 (*Ecm1*) and matrix metalloproteinase 2 (*Mmp2*) were higher in aged hamsters than in young hamsters (Figure 2g). The above data pointed to an unresolved disease in aged hamsters. Altogether, young and aged hamsters respond differently to SARS-CoV-2-infection (acute and resolving phases), with a more severe and persistent disease in aged animals.

SARS-CoV-2 infection differentially affects gut microbiota composition and function in young and aged hamsters

We then compared the gut microbiota composition and function in SARS-CoV-2-infected young and aged hamsters by analyzing cecal contents on D7 and D22 (n = 3–6/group). No significant changes in alpha diversity (Shannon index, genus level) were observed between the experimental groups (Supplementary Figure S3a). However, PCoA based on Aitchison distance (species level) revealed significant alterations in the microbiota community structure in both age groups on D7 (Figure 3(a)p = 0.006 and R2 = 0.35 for D7 aged vs D0 aged; p = 0.016 and R2 = 0.28 for D7 young vs D0 young). On D22, the bacterial community structure shifted toward the baseline groups, but remained distinct from baseline in both aged (p = 0.016 and R2 = 0.31 for D22 aged vs D0 aged; p = 0.039 and R2 = 0.33 for D22 aged vs D7 aged) and young animals (p = 0.016 and R2 = 0.22 for

was sacrificed. Lower panel, difference at D22 is shown. c, Histopathological examination of lung sections (H&E staining). Total score is indicated for each group. d, volcano plot of transcriptomic data generated from whole lung tissue collected from young and aged hamsters (D7). The x-axis represents the -log2 fold change for differentially expressed genes in mock vs. infected lungs, and the y-axis represents the -log10 (p.Adj). Significant differentially expressed genes in infected lungs with a fold change threshold of 0.6 (vertical dashed lines) and a *P*-value <0.05 (horizontal dashed line) are shown in red (for upregulation) or blue (for downregulation). e, Gene set enrichment analysis from Kyoto Encyclopedia of genes and genomes (KEEG) and keywords biological process (KW_BP) (aged hamsters, D7). f, *left* panel: sirius red staining images. *right* panel: percentage of sirius red labeling in lungs on D22. g, expression of *Col1a1*, *Col3a1*, *Ecm1* and *Mmp2* gene expression in lungs from young and aged hamsters on D22 by quantitative RT-PCR. The data are expressed as the mean fold change relative to average gene expression in mock-infected young animals (6 young hamsters and 3 aged hamsters). a-c, f and g, n = 3–6/group. d and e, n = 4/group. Significant differences were determined using the two-way ANOVA (uncorrected Fisher's LSD; mixed-effects analysis) test (b, upper panel) and the Mann Whitney U test (a, left panel, b, lower panel, c, f, left panel and g) (*p < 0.05; **p < 0.01, ****p < 0.0001).
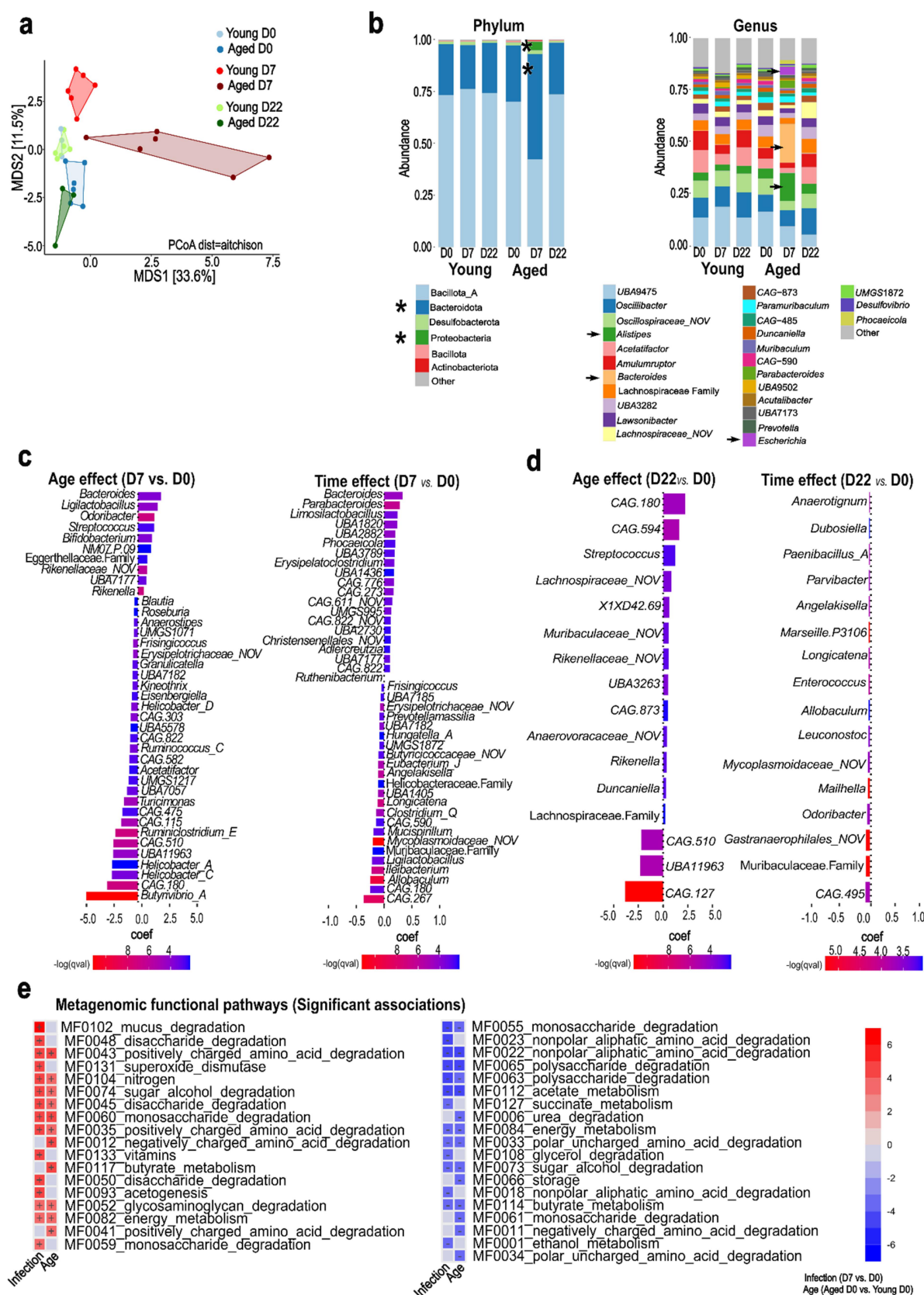
Figure 3. Taxonomic and functional profile of the gut microbiota across different age groups and infection states. a, PCoA plot (species) of β-diversity based on Aitchison distance metric, differentiating infection status (non-infected: blue, D7: red, D22: green) and age group (young: light colors, aged: dark colors). b, compositional bar plots illustrating the taxonomic profile of gut microbiota at the phylum (*left* panel) and genus (*right* panel) levels. The relative abundance of each taxon is represented by the bar height. Asterisks and

D22 young vs D0 young; $p = 0.006$ and R2 = 0.27 for D22 young vs D7 young). On D7, aged hamsters exhibited the most pronounced shifts in microbiota composition, including a marked increase in the relative abundance of the Bacteroidota phylum (from 27% to 47%) and the Pseudomonadota phylum (from 0.05% to 3%) (Figure 3(b), *left* panel). Within the Bacteroidota, the genera *Alistipes* and *Bacteroides* increased significantly, whereas within Pseudomonadota, the *Escherichia* genus showed a significant rise (Figure 3(b), *right* panel and Supplementary Figure S3b).

We next employed a multivariate linear model to identify statistically significant associations between gut microbial taxa and animal metadata (age and day of infection). Between D0 and D7, aged hamsters showed significant positive associations with genera such as *Bacteroides*, *Ligilactobacillus*, *Odoribacter*, *Streptococcus*, and *Bifidobacterium* (Figure 3(c)). In contrast, the young group was enriched with genera including *Butyrivibrio_A*, *Ruminiclostridium_E*, *Ruminococcus_C*, and certain *Helicobacter* groups. For the time variable, several genera like *Bacteroides*, *Parabacteroides*, *Limosilactobacillus*, *Phocaeicola*, and *Erysipelatoclostridium*, increased on D7, whereas others such as *Allobaculum*, *Ileibacterium*, and *Ligilactobacillus* decreased. Between D0 and D22, fewer significant associations were found. Age was positively associated with the genera *CAG.180 (f__Acutalibacteraceae)*, *CAG.594 (c__Bacilli)*, and *Streptococcus*, and negatively associated with CAG-127 (f__Lachnospiraceae), UBA11963 (c__Bacilli) and CAG-510 (f__Lachnospiraceae) (Figure 3(d)). Time negatively associated with CAG-495 (c__Alphaproteobacteria), *Odoribacter*, *Mailhella*, and other genera (Figure 3(d)).

To elucidate the functional implications of microbiota alterations, we conducted a multi-step metagenomic functional analysis incorporating HUMAnN,[56] GOmixer, and MaAsLin2.[57] During the acute phase of infection (D7), significant modulations in gut metabolic modules were identified, which were associated with age and infection status (Figure 3(e)). Specifically, the acute phase of infection was characterized by the upregulation of modules involved in mucus degradation, simple carbohydrate degradation, and positively charged amino acid degradation on D7. There was also an increase in modules related to nitrogen metabolism, vitamin metabolism, energy metabolism, superoxide dismutase activity, and acetogenesis (Figure 3(e)). Interestingly, there was a downregulation of some carbohydrate degradation modules (mainly polysaccharides), nonpolar amino acid degradation, and SCFA metabolism (acetate and butyrate) (Figure 3(e)). These findings suggest a dynamic shift in gut microbiota function during the early stages of infection. In comparison, the resolving phase of infection (D22) showed a downregulation of carbohydrate and amino acid degradation modules (Supplementary Figure S3c). Conversely, there was an upregulation of modules related to ethanol and energy metabolism, indicating a shift in resource allocation or altered energy demands during recovery. The analysis of age effects also revealed contrasting patterns between the acute and resolving phases. During the acute phase, age was positively associated with charged amino acid degradation, saccharide degradation, and butyrate metabolism, and negatively associated with overall amino acid degradation, saccharide degradation (including more complex carbohydrates), urea degradation, and acetate and butyrate metabolism (Figure 3(e)). In the resolving phase (D22, Supplementary Figure S3c), age was negatively associated with monosaccharide degradation and

arrows indicate major changes between D0 and D7. c, MaAsLin2 multivariate differential abundance analysis for bacterial genera comparing D7 with non-infected controls, stratified by age group (young and aged). d, MaAsLin2 multivariate differential abundance analysis for bacterial genera comparing D22 with non-infected controls, stratified by age group (young and aged). c-d, *left panel*: bar plot depicting the age effect, with positive coefficient values indicating bacterial genera that are significantly enriched in aged animals compared to young animals. *right panel*: bar plot depicting the time effect, with positive coefficient values indicating bacterial genera that are significantly enriched in infected (D7 or D22) animals compared to non-infected controls. e, MaAsLin2 multivariate differential analysis for gut microbiota functional pathways represented as a heatmap with columns for both the infection and age effects. Positive values (red) indicate enrichment in infected or aged groups.

SCFA metabolism, and positively associated with the degradation of more complex carbohydrates and charged amino acids. This finding suggests an age-dependent modulation of microbiota metabolic pathways during recovery.

SARS-CoV-2 infection differentially alters plasma metabolite concentrations in young and aged hamsters

Clinical studies demonstrated the good discriminatory power for distinguishing COVID-19 disease severity based solely on a selection of circulating metabolites.[19,23,58–60] We hypothesized that the aging model used in the current study, characterized by gut dysbiosis, high infection level, and pronounced lungs sequelae, may exhibit a specific profile of plasma metabolome serving as biomarkers of disease severity. To test this hypothesis, we compared the plasma metabolite levels in young and aged hamsters during SARS-CoV-2 infection ($n = 3$–6/group). PCoA revealed that infection significantly impacted plasma metabolite concentrations on D7 in aged hamsters, with some differences persisting until D22 (Figure 4(a)). Several of these metabolites were associated with microbial metabolism.[45,61] ANOVA-Simultaneous Component Analysis (ASCA) with permutation testing revealed significant differences between experimental groups based on age ($p < 0.05$) and infection status ($p < 0.05$) (Supplementary Figure S4a), although no significant interaction between these variables was found. Using multivariate analysis with random forest, we identified the 15 most relevant variables for discriminating between experimental groups. This list encompassed metabolites such as cis-aconitic acid, citric acid, spermidine, and various amino acids and their derivatives, including kynurenine, creatine, glutamic acid, tryptophan, phenylalanine, proline betaine, 2-aminobutyric, serine, trans-4-hydroxyproline, and 1-methylhistidine (Figure 4(b)). Choline and the bacterial product trimethylamine (TMA) were also among the top 15 discriminating metabolites. Hierarchical clustering of the top 30 metabolites revealed two distinct clusters (Figure 4(c)). The first cluster contained metabolites with high concentrations on D7 in aged hamsters, some of which returned to baseline levels on D22 (e.g.,

1-methylhistidine, kynurenine, L-carnitine, p-cresol sulfate, 2-aminobutyric acid). This cluster also included sarcosine and cis-aconitic acid, which remained elevated on D22. Notably, some metabolites within this cluster, such as cysteine, creatine, indoxyl sulfate, and spermidine, were reduced in young animals on D7. The second cluster comprised metabolites with reduced concentrations on D7 in young, aged, or both groups. Some, like citric acid and indole-3-propionic acid, returned to baseline levels on D22. However, tryptophan, phenylalanine, and glutamic acid remained low on D22, particularly in aged animals (Figure 4(c)).

We then employed a Two-Way ANOVA test within a univariate statistical framework to investigate the impact of age, infection, and their interaction on metabolite levels. Age emerged as a crucial factor contributing to the elevation of 1-methylhistidine (transient increase in aged animals) (Figure 4(d) and Supplementary Figure S4a). Interestingly, this metabolite has been identified as a predictor of survival chances in hospitalized COVID-19 patients with average age more than 79 years.[58] Notably, SARS-CoV-2 infection induced significant alterations in nine metabolites independently of age on D7. While citric acid, kynurenine, and 2-aminobutyric acid returned to basal levels by D22, metabolites like cis-aconitic acid, choline, and sarcosine showed sustained alterations in both young and aged groups on D22 (non-infected vs. D7, $p < 0.05$ and non-infected vs. D22, $p < 0.05$ for all age groups). Exploring metabolites associated with the prolonged effects of infection, we observed that tryptophan, phenylalanine and glutamic acid remained altered on D22 only in aged hamsters (non-infected vs. D22, $p < 0.05$ for the aged group) (Figure 4(d)). Using Enrichment Global Test and Topology analysis, we verified how the significant metabolites (altered after acute or long infection regardless of age) interact and connect with each other, respectively. The interaction shown in the metabolite sets enrichment overview revealed that SARS-CoV-2 infection mainly alters the metabolism of key amino acids, energetic pathways, and cell membrane components (Supplementary Figure S4b). The network plot further reinforced the relationship between these pathways (Supplementary Figure S4c). In summary, SARS-CoV-2 infection
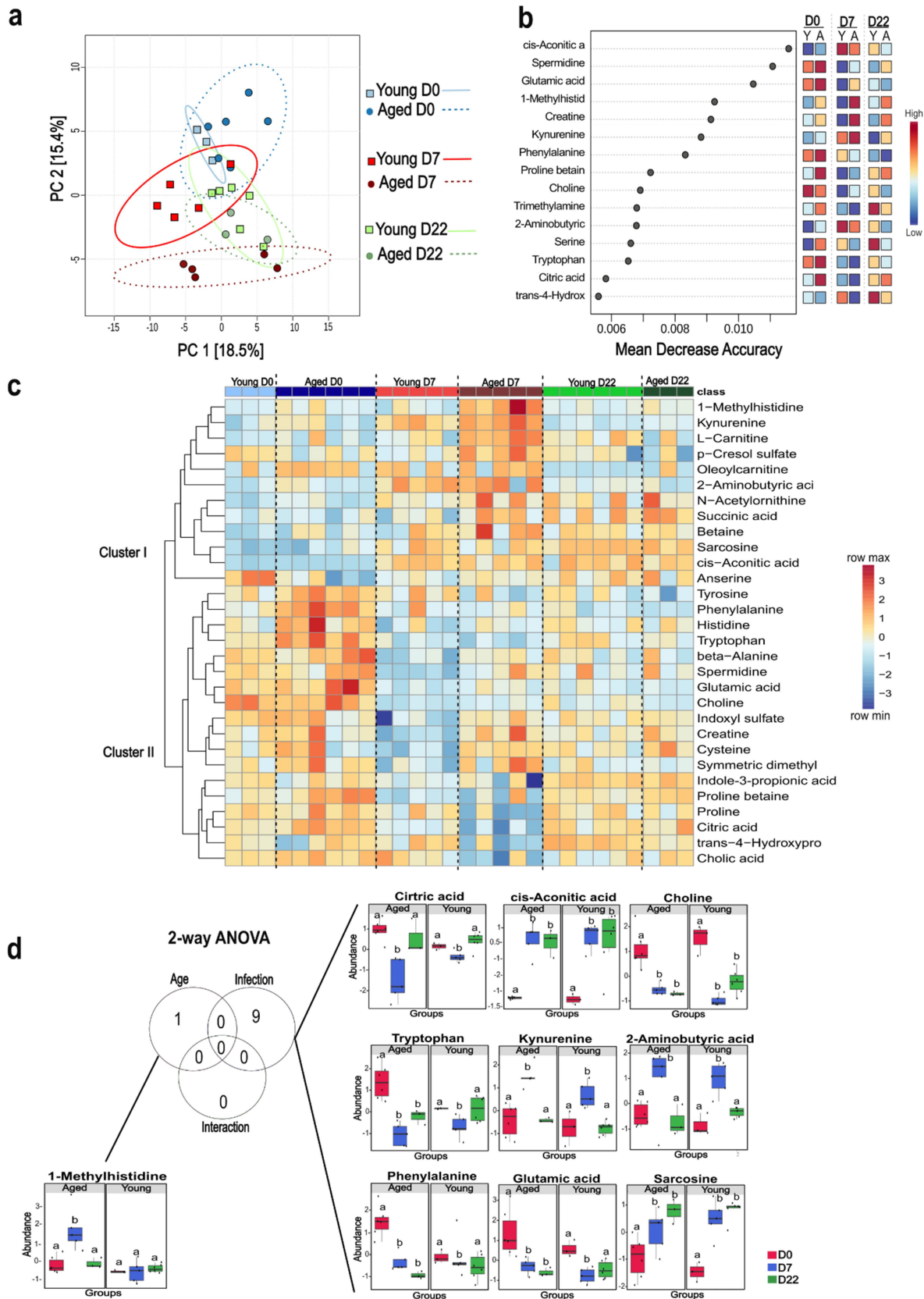
Figure 4. Multivariate and univariate analyses, and metabolite sets enrichment overview of plasma metabolome profiles of SARS-CoV-2-infected young and aged hamsters. plasma metabolomic profiling of mock-infected and SARS-CoV-2-infected young and aged hamsters on D7 and D22. Shown are the multivariate analysis with PCA. [PERMANOVA] F-value: 6.3905; R-squared: 0.59223; p-value (based on 999 permutations): 0.001) (a) and ranking of top 15 metabolites identified by random forest, based on mean decrease

differentially modulates systemic metabolite concentrations in young and aged hamsters, revealing age-dependent metabolic responses to infection. It is noteworthy that SARS-CoV-2 infection has long-term effects in both age groups, with some changes being specific to aged hamsters.

Microbiota taxa and metabolites associate differently with acute disease markers in young and aged hamsters

We then performed an integrative analysis combining metagenomics, metabolomics and clinical data to identify relevant associations (Supplementary Table S3). Using Hierarchical All-against-All (HAllA) association testing, we explored pairs of datasets, applying the Spearman correlation coefficient to measure associations for continuous data. Significant associations were visualized as networks, where each node represented a feature (metabolite, bacterial species, or infection marker) and each edge indicated a correlation between two different features. By comparing the D7 groups with non-infected controls, we generated two distinct networks for young and aged hamsters (Figure 5). Compared to young hamsters, aged hamsters exhibited a denser network of correlations (70 edges vs. 21 edges). In aged hamsters, amino acids, including proline, isoleucine, serine, methionine, valine, tyrosine, phenylalanine, histidine, tryptophan, and glutamic acid, showed positive correlations with body weight and/or lung barrier integrity (*Zo1*), and negative correlations with virus copy numbers, pneumonia score, *Cxcl10* and/or *Ccl2* (Figure 5(a) and Supplementary Figure S5). The gut bacteria species *Alistipes_sp003979135* and *D16-63_MGBC165261* (f__Eggerthellaceae) were positively associated with some of these amino acids. Other metabolites, such as histamine, L-acetylcarnitine, choline, and citric acid presented similar correlation patterns. Furthermore, proline betaine and the bile acid

tauromuricholic acid correlated positively with body weight, while indoleacetic acid, cholic acid, and creatine correlated negatively with the pneumonia score. Indoleacetic acid also correlated negatively with virus copy numbers (Figure 5(a)). Associations between bacterial taxa and metabolites were also observed in the aged group on D7, although we noticed a lack of direct correlation between taxa and disease markers. *Bacteroides thetaiotaomicron* and proline betaine showed a negative correlation, while *UBA1394* (f__Ruminococcaceae) was positively correlated with L-acetylcarnitine, and three other *UBA11940* (f__Borkfalkiaceae) species were positively correlated with indoleacetic acid (Figure 5(a)). In young hamsters, a distinct profile emerged, with virus copy number correlating negatively with carnosine, beta-alanine, and *COE1_sp002358575* (Lachnospiraceae family) (Figure 5(b)). Another species of the Lachnospiraceae family, *COE1_MGBC117419*, and carnosine, correlated negatively with pneumonia score. Furthermore, cis-aconitic acid correlated negatively with body weight and *Zo1*, the later positively associated with Eubacterium, Lawsonibacter and Oscillospiraceae. Body weight also presented negative correlation with *Turicimonas muris* and positive correlation with *Lawsonibacter_MGBC000538* and *UBA7182_MGBC119923* (f__Lachnospiraceae (Figure 5(b)). Overall, our findings reveal distinct metabolic and microbial associations during SARS-CoV-2 infection between young and aged hamsters on D7.

Amino acids and specific metabolites emerged as key indicators of disease progression in aged animals

In our experimental settings, aging favors non-resolving damage following SARS-CoV-2 infection, including delayed body weight recovery (Figure 2(b) and Supplementary Figure S2a), development of lung fibrosis (Figure 2(f–g)) and

---

accuracy (b). Colored boxes indicate relative concentrations of metabolites in each group, c, hierarchical cluster analysis and heatmap of top 30 metabolites selected based on raw *P*-value from the one-way ANOVA. Clustering was performed using the average method with Euclidean distances as the metric. Each colored cell on the map corresponds to a normalized metabolite concentration, with metabolites name in rows and samples in columns. Young=light blue; Aged=dark blue; infected D7 young=red and aged=dark red; infected D22 young =light green and aged=dark green. Note the elevated ratio between kynurenine (high) and tryptophan (low) at D7, a feature of the acute phase. d, univariate analysis via two-way ANOVA (threshold FDR *p* < 0.05) with Tukey's posttest comparing infected vs. non-infected control for both age groups. Non-infected=red; infected D7=blue and infected D22=green.
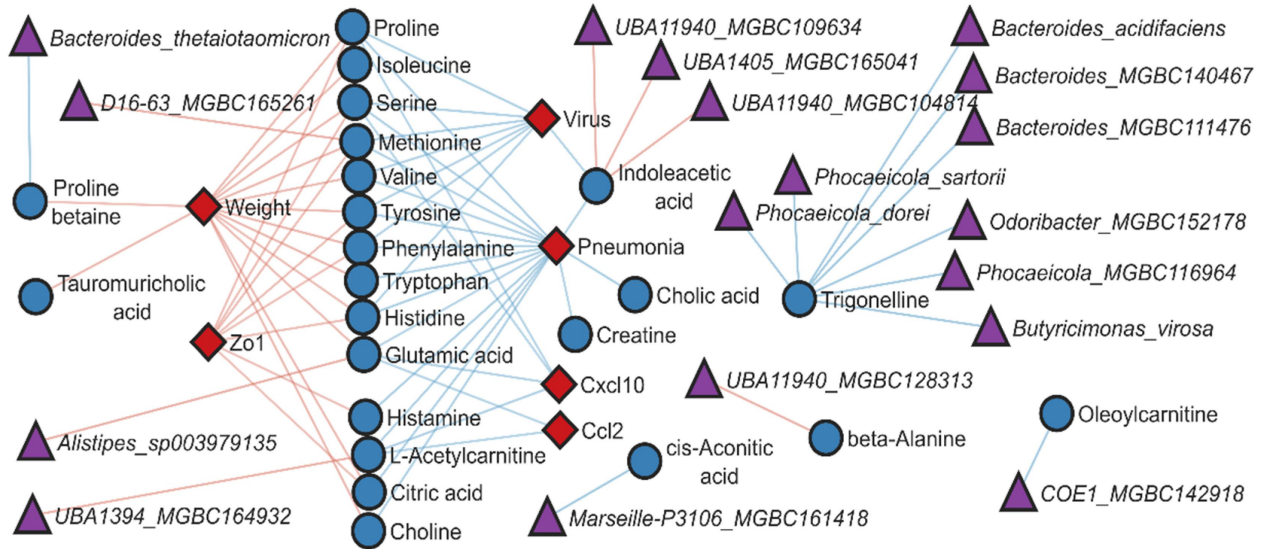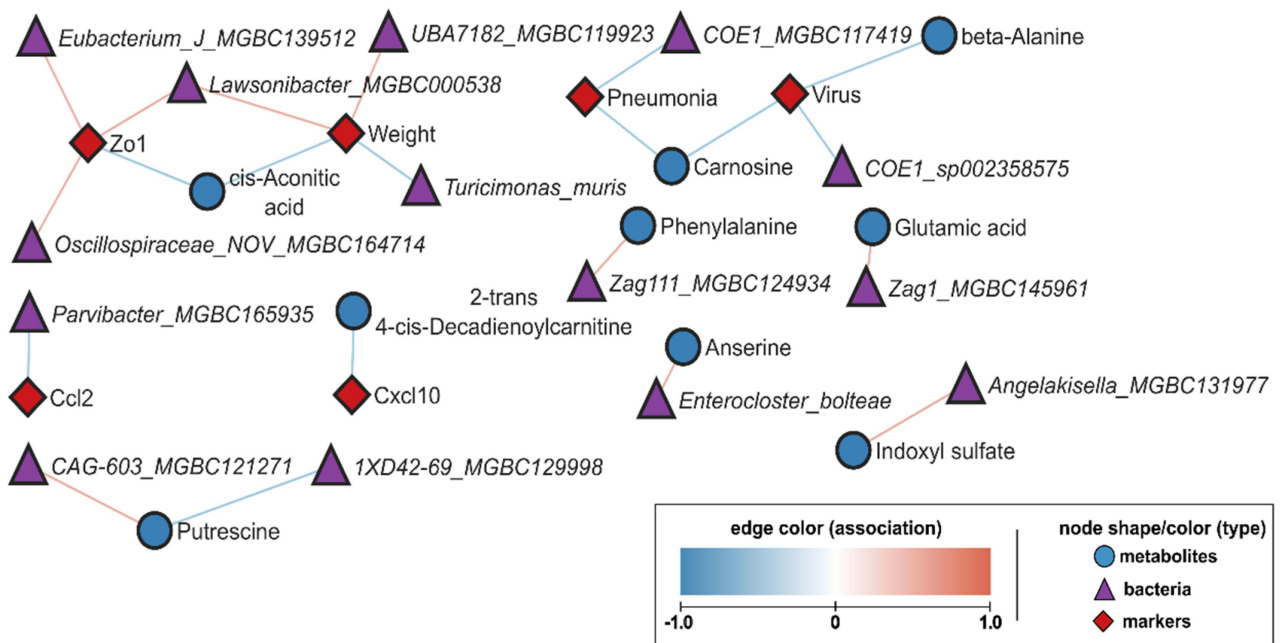
Figure 5. Correlation between systemic metabolites, taxa and early infection-related variables (D0 *vs* D7). a and b, continuous data from hamsters infected with SARS-CoV-2 (D7 and non-infected controls) were used to calculate Spearman correlation coefficient, with adjusted *P*-value ≤ 0.05. Each node represents a biological entity (metabolites, gene, bacterial species, or infection markers). Edges represent statistically significant associations between the connected nodes of different types, with red edges for positive and blue edges for negative correlation. a, network for aged hamsters. The correlation network centered around amino acids and some of their derivative molecules with positive association with body weight and negative association with viral load and inflammation. b, network for young hamsters.

persistent changes in metabolites potentially linking host and microbiota metabolism (Figures 4(d)). We therefore analyzed potential correlations between these disease markers, metabolites and microbiota changes on D22. For that purpose, we compared the D22 group to non-infected controls and generated distinct networks for young and aged hamsters (Figure (6)). In aged hamsters, body weight correlated positively with several amino acids (tyrosine, tryptophan, phenylalanine,
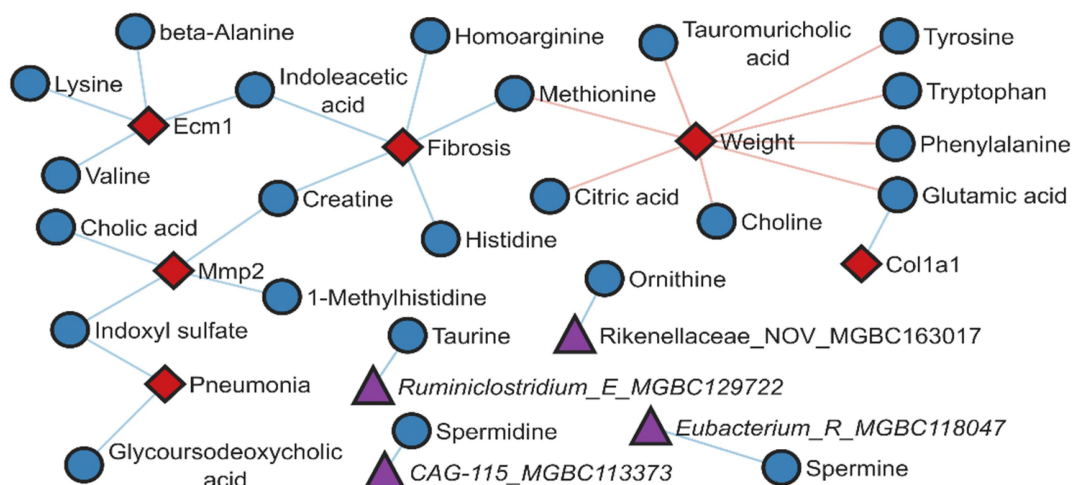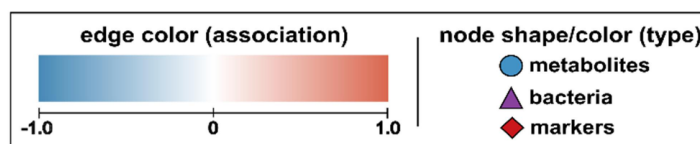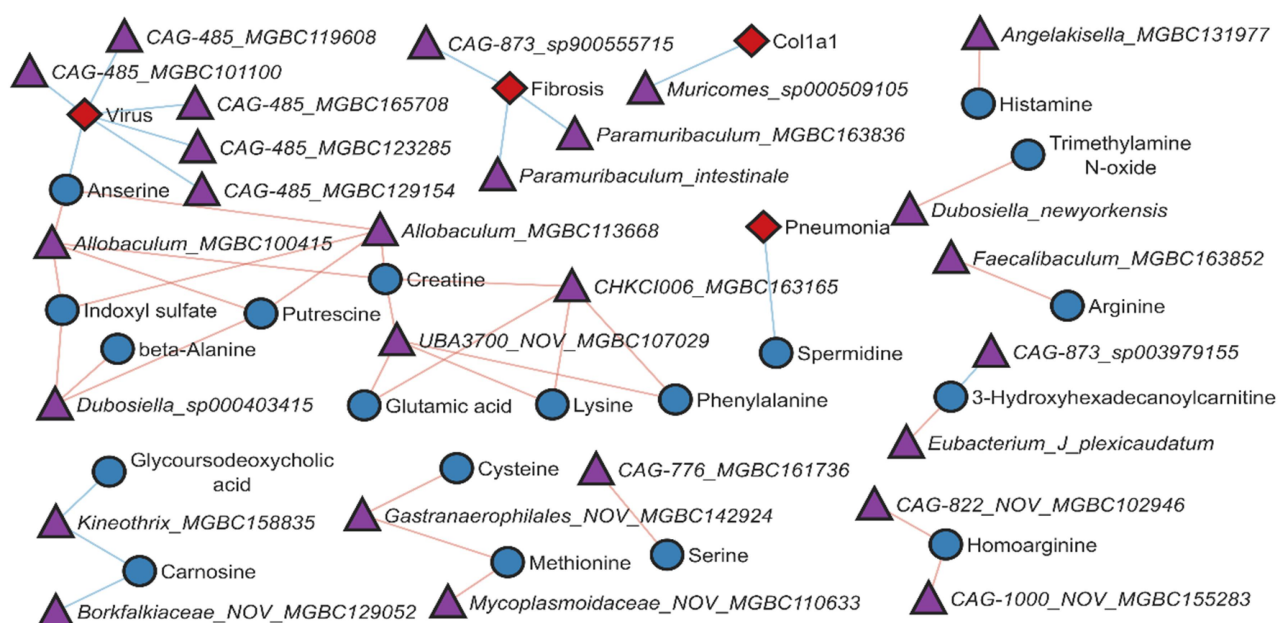
a aged hamsters, D0-D22 (33 nodes, 28 edges)

b young hamsters, D0-D22 (49 nodes, 44 edges)

Figure 6. Correlation between systemic metabolites, taxa and late infection-related variables (D0 *vs* D22). a, network for aged hamsters. **b**, network for young hamsters. **a** and **b**, continuous data from hamsters infected with SARS-CoV-2 (D22 and non-infected controls) were used to calculate Spearman correlation coefficient, with adjusted *P*-value ≤0.05. Each node represents a biological entity (metabolites, gene, bacterial species, or infection markers). Edges represent statistically significant associations between the connected nodes of different types, with red edges for positive and blue edges for negative correlation.

glutamic acid and methionine), as well as with choline, citric acid and tauromuricholic acid (Figure 6(a) and Supplementary Figure S6). Conversely, fibrosis correlated negatively with methionine, histidine, homoarginine, creatine and indoleacetic acid. Other metabolites like indoxyl sulfate, 1-methylhistidine, cholic acid, valine, lysine, beta-alanine, indoleacetic acid and glutamic

acid correlated negatively with the fibrosis marker genes *Mmp2*, *Ecm1* and/or *Col1a1* (Figure 6(a)). It is noteworthy that on D22, no bacterial taxa associated with body weight and fibrosis in aged animals. In the young group, some bacterial species (from the *Paramuribaculum* and CAG485 genera) and metabolites (anserine) correlated negatively with fibrosis, suggesting a possible role of these components in the recovery phase. Apart from that, limited correlation between bacterial species and/or metabolites and disease markers were observed in young animals on D22. Overall, some amino acids and specific metabolites emerged as key indicators of disease progression in aged animals, with strong associations with body weight and fibrosis.

Discussion

Clinical studies have evidenced changes in gut microbiota composition during SARS-CoV-2 infection,[9,11–14,20,22,23] this alteration can persist for many months.[10,16–19,21,24] However, metagenomic characterization for advanced age individuals remains elusive. Since clinical studies typically involved hospitalized patients, it is challenging to distinguish between the direct effects of the viral infection and the impacts of hospitalization and medication on the metagenomics results. Therefore, preclinical models are instrumental to analyze the potential impact of advanced age on virus-induced dysbiosis and on subsequent disease outcomes. In the present study, we took advantage of a Syrian hamster model recently described to simulate the clinical and pathological manifestations of COVID-19.[25,26,52] We used high-throughput shotgun metagenomics and metabolomics analyses to identify potential bacterial and metabolite markers of acute and long-term COVID-19 in aged hamsters, revealing the impact of aging on gut microbiota composition and disease outcomes.

In the absence of infection, we found altered microbiota composition in 22-month-old hamsters (~80 years old for humans), as indicated by beta diversity analysis. Aged hamsters showed enrichment in the order *Lactobacillales* and species including *Bifidobacterium animalis* and *Ligilactobacillus murinus*, and *Alistipes* genus.

Lactobacillales and *Bifidobacterium* species are abundant in healthy elderly individuals.[62,63] In mice, *B. animalis* is positively associated with longevity[64] and/or good health.[65,66] The *Alistipes* genus has also been reported to increase in the gut microbiota of aged individuals, despite some controversial observations.[28,67] These findings suggest that our aged non-infected hamsters may represent a model of healthy elderly gut microbiota. Regarding systemic metabolic output, anserine and p-cresol sulfate levels were reduced in the plasma of aged hamsters compared to young hamsters. Anserine, a natural carnosine derivative, possesses anti-inflammatory and antioxidant properties that are dependent on gut microbiota.[47] The decline in anserine levels with age may be due to multiple factors, including changes in the digestion and absorption of dietary nutrients,[68] as seen in aged mice.[69] Anserine supplementation has been linked to improvements in cognitive and inflammatory processes during aging.[70,71] p-cresol sulfate is the fermentation product of p-cresol, a gut microbiota-derived product of L-tyrosine.[46] It also has anti-inflammatory properties, including in the lungs.[72] To the best of our knowledge, its concentration in aged plasma (in rodents and others) has not yet been described. Based on these findings, and in line with observations in other species,[28] aged hamsters exhibit alterations in both the composition and functionality of the gut microbiota under steady-state conditions. These changes may play a role in shaping the host response to infection. Indeed, compared to young animals, aged hamsters showed higher viral loads and experienced unresolved disease (more intense and prolonged weight loss and greater pulmonary fibrosis) following SARS-CoV-2 infection. Our RNAseq analysis suggested that the heightened activation of proteasome and immune pathways observed in aged hamsters may explain worse disease outcomes. Whether preexisting gut dysbiosis distally affects lung defense, body weight recovery and/or lung fibrosis in aged individuals remains to be demonstrated. Further experimental exploration, including fecal transfer experiments, is required to investigate this issue.

The influence of the age on virus-induced gut dysbiosis was then assessed. Our data show that SARS-CoV-2 infection elicited more pronounced

alterations in the gut microbiota of aged hamsters compared to young hamsters. In aged hamsters, the genera *Bacteroides*, *Ligilactobacillus*, *Odoribacter*, *Streptococcus*, and *Bifidobacterium* increased while in the young group, *Butyrivibrio_A*, *Ruminiclostridium_E*, *Ruminococcus_C*, and certain *Helicobacter* groups were more abundant. Taxonomic changes were relatively transient, although some genera showed persistent alterations in the aged group. These include the detrimental genera *Streptococcus* (increased) and members of the beneficial, SCFA producer family Lachnospiraceae (CAG-127 and CAG-510) (decreased). More research is also required to better understand the role of these species in different phases of COVID-19 such as the acute inflammatory phase and the subsequent periods of resolution and tissue repair. To address this gap, fecal transfer experiments would be necessary. It is noteworthy that this approach is instrumental to study the consequences of virus-induced dysbiosis on the early and later outcomes of respiratory viral infections.[73,74] Functional analysis of metagenomics data revealed that several microbial metabolic pathways were altered during infection, many of which were also affected by aging. Notably, there was an increase in pathways related to energy metabolism, degradation of monosaccharides and disaccharides, and degradation of positively charged amino acids. At the same time, pathways involved in polysaccharide degradation were reduced. Both aged and young hamsters showed a reduction in SCFA (acetate and butyrate) production pathways after infection. This is in line with the reduced frequencies of SCFA producers such as *Butyrivibrio_A*, *Ruminiclostridium_E*, and *Ruminococcus_C* in infected aged animals (the current study). Reduced SCFA production during acute respiratory infection has been reported in preclinical and clinical studies.[16,26,37,73,75–77] These gut microbiota functional alterations induced by infection, along with other age-associated changes, may contribute to the worsened response to SARS-CoV-2 infection in aged individuals. Aging plays a significant role in the long-term impact of infection. At D22, aged hamsters showed a negative association with butyrate and acetate metabolism pathways. Reduction of SCFA metabolism is a hallmark of aged individuals[28] and a marker of

long COVID-19 in humans.[77] Moreover, and in line for our metabolic analysis, age was positively associated with the degradation of amino acids during the acute and recovery phases of infection. Together, our metagenomics analysis demonstrates that SARS-CoV-2 infection triggers a pronounced perturbation of the gut microbiota's composition and function in aged individuals. Of note, this finding was recently confirmed using a metaproteomics approach (Creskey and *al.*, submitted).

SARS-CoV-2 infection significantly impacts on metabolite levels in both young and aged hamsters, but the types of metabolites and their clustering patterns, associated with microbiota composition and disease markers, differed between the age groups. For example, aged hamsters exhibited a transient elevation in 1-methylhistidine, a product of histidine methylation associated with muscle protein turnover and metabolism,[78] body weight loss, and sarcopenia.[79] As metabolic disorders and sarcopenia significantly affected hospital outcomes and increased the risk of physical decline post-COVID-19 recovery,[80–82] systemic 1-methylhistidine in patients might serve as a valuable prognostic factor.[58] Of interest, patients with severe/critical COVID-19 have significantly elevated levels of 1--methylhistidine.[59] By integrating our various omics data, we identified associations between the gut microbiota, metabolome, and infection markers. Several amino acids (phenylalanine, tryptophan, glutamic acid) and indoleacetic acid emerged as potential protective factors during both the acute and resolving phases of SARS-CoV-2 infection in aged hamsters. For instance, the sustained drop of tryptophan, phenylalanine, and glutamic acid correlated with the lack of body weight recovery in aged animals on D22. In severe COVID-19 cases, patients in intensive care units show increased degradation of these amino acids due to heightened gluconeogenesis and lipid breakdown,[59,83,84] which is associated with COVID-19 outcomes.[19,59] More studies are needed to investigate the pathways involved in these changes and to identify potential treatment targets to reduce the impact of infection on amino acid metabolism and protein turnover. These metabolites warrant further testing as possible prognostic markers for severe/critical COVID-19 cases. Our data suggest the importance of prolonged monitoring of elderly individuals,

especially regarding nutritional support of amino acids. The tryptophan metabolite indoleacetic acid also negatively associated with key disease markers at D7 and D22 in aged animals. This microbiota-derived metabolite (reduced concentration) has previously been associated with SARS-CoV-2 infection in humans[60,85] and is well described for its anti-inflammatory and tissue protective role, including in the lungs.[86–88] It is noteworthy that reduced indole-3-propionic acid, another microbial tryptophan metabolite, also correlated with disease outcome during viral pneumonia.[19,37,89] In young hamsters, carnosine may act as a potential protective factor, while cis-aconitic acid appears as a potential acute disease marker on D7. In the aged group, bacterial taxa did not directly correlate with disease markers on D7 and D22. However, based on indirect associations, some gut microbiota components such as *Alistipes_sp003979135* (glutamic acid), *D16-63_MGBC165261* (f__Eggerthellaceae) (methionine) and UBA11940/UBA1405 (f __Borkfalkiaceae) (indolacetic acid) may be beneficial during the acute phase. In young hamsters, different species including members of Eubacterium, Lawsonibacter, Oscillospiraceae, COE1 (f__Lachnospiraceae), and UBA7182 (f__Lachnospiraceae) were associated with disease severity and may provide protection on the acute phase of infection in young hamsters. Other species such as *Paramuribaculum* and CAGs may also be protective, but on the resolving phase of the infection (D22).

In the current study, we experimentally assessed gut microbiota changes and their associations with systemic metabolites, disease severity markers across two different ages and at different time points post-infection (acute and recovery phases). The current study provides several links between aging, gut microbiota components, metabolites, and the response to infection and supports the development of age-adapted, personalized micro-biome-targeting strategies (nutritional, pre/pro/postbiotics) to manage disease outcomes. However, the study also had some limitations. First, the hamster model does not replicate all the features of severe COVID-19; the hamster rapidly resolves the COVID-19-like disease, although post-acute sequelae persist.[52,90] Moreover, compared to severe COVID-19 patients, the hamster model is less relevant when referred to gut disorders. Therefore, translating these results from animal models to human physiology demands caution. Moreover, this study involves small sample sizes, limiting generalizability. The data provided in the current study need confirmation with a higher number of animals. The use of other experimental models of aging (*e.g.* aged mice using a murinized strain of the virus) would be interesting. Another limitation that must be acknowledged pertains to our metabolomics analysis, which, due to the large volume of plasma required, did not include SCFAs. Moreover, SCFA levels were not quantified in fecal or cecal samples. Given the key role of SCFAs in health and disease and the impact of respiratory viral infections on SCFA levels,[26,39] SCFAs might correlate with disease markers in aged hamsters, as suggested in humans.[16,77] Lastly, while our study provides insights into potential protective metabolites and bacterial taxa, correlation does not imply causation, warranting cautious interpretation. More research (preclinical models and clinical studies) is therefore necessary to characterize and validate biomarkers that can predict the course of viral pneumonia in the aged population, with the ultimate goal of reducing critical complications. Functional studies are also requested to experimentally test the potential effects of candidate metabolites, such as certain amino acids, indoleacetic acid and 1-methylhistidine, in the COVID-19-like severity. Despite these limitations, our study provides the first description of gut microbiota changes during experimental severe COVID-19 in aged hamsters. Identifying factors contributing to the severity of COVID-19, as well as other acute respiratory viral infections such as influenza, in elderly individuals is a first step toward developing more personalized therapies for this condition in order to reduce the risk of death and lower long-term sequelae. In this context, the dysregulation of gut microbiota, expressed by an altered profile of (microbial) metabolites, underscores the potential relevance of dietary interventions to more effectively manage the long-term outcomes of acute viral pneumonia in the aged population.

Material and methods

Animals and ethics statement

Golden Syrian hamsters were purchased from Janvier Laboratory (Le Genest-Saint-Isle, France). Hamsters aged 2 months (young group) and 22 months (aged group) were provided with standard rodent chow (SAFE® A04, Augy, France) and water *ad libitum* throughout experiments (3 hamsters/ cage). All animal protocols were reviewed and approved by the local ethics committee "Comité d'Ethique en Expérimentation Animale" (CEEA) Nord/Pas-de-Calais 75. The study was authorized by the "Education, Research and Innovation Ministry" under registration number APAFIS#25041–2020040917227851 v3.

Infection with SARS-CoV-2

Experiments involving live SARS-CoV-2 were conducted in the biosafety level 3 laboratory (BSL3) within the Institut Pasteur de Lille, adhering to national and institutional regulations and ethical guidelines (Institut Pasteur de Lille/B59–350009). After a 7-day acclimation in isolators within the BSL3 facility, hamsters were anesthetized with intraperitoneal injections of ketamine (100 mg/ kg), atropine (0.75 mg/kg), and valium (2.5 mg/ kg). Hamsters ($n = 16$–18) were then intranasally infected with 100 µl of DMEM, containing either 2×10^4 TCID50 of SARS-CoV-2 (BetaCoV/France/ IDF/0372/2020) for infected animals or DMEM alone for non-infected control animals. Body weight was monitored before and during infection. For tissue collection, animals were euthanized with an intraperitoneal injection of euthasol (140 mg/ kg). Blood, lungs, and feces were collected from non-infected (day 0 (D0)) and SARS-CoV -2-infected hamsters on D3, D7, and D22 (3 to 6 animals per group).

Quantification of viral load, determination of gene expression and histopathological assessments

Quantification of viral load and determination of gene expression in lungs were performed by quantitative, SYBR Green-based, RT-PCR (whole lung tissue) as described.[37] Individual mRNAs were quantified relative to the expression of genes coding for RNA-dependent RNA polymerase (RdRp) and gamma actin (Actg1). The viral load was expressed as the amount of viral RNA relative to *Actg1* expression level ($\triangle$Ct). For host gene expression, relative mRNA levels were determined according to the $2^{-\Delta\Delta}$Ct (cycle thresholds) method. Data were normalized against the expression of the *Gapdh g*ene and expressed as fold-change over the mean gene expression level in mock-treated mice.[37] Specific primers are shown in Supplementary Table 4. The detection of SARS-CoV-2 in lung sections was performed as described in.[52] Histopathologic scores of lung sections were determined using hematoxylin and eosin (H&E) reagent and criteria defined in.[44] To quantify pulmonary fibrosis, lung sections were stained with Sirius Red. Stained areas were measured with a computer-assisted, automated, whole-section histomorphometric image analysis technique (Visiopharm, Hørsholm, Denmark).[52]

RNA sequencing analysis and statistical analysis

RNA quality was evaluated by spectrophotometry (Nanodrop, Thermo Fisher), RIN (Bioanalyzer 1200, Agilent Technologies), and quantified by fluorimetry (Qubit, Thermo Fisher). Libraries were prepared from 200 ng of total RNA using the QIAseq stranded mRNA library kit (Qiagen), according to the manufacturer's protocol (n = 3–4/ group). Libraries were controlled using the Bioanalyzer 1200 (Agilent Technologies) and quantified by quantitative PCR (KAPA Library Quantification Kit for Illumina platforms, KapaBiosystems). Libraries were normalized and pooled equimolarly before sequencing on a NovaSeq sequencer (Illumina) in 2×150 bp mode. Raw sequencing datasets were analyzed using the nf-core/rnaseq v3.6 pipeline.[90] Raw FastQ files were quality and adapter trimmed with Trim Galore v0.6.7. (https://www.bioinformatics. babraham.ac.uk/projects/trim_galore/). Ribosomal RNA reads were filtered with SortMeRNA v 4.3.4. Cleaned reads were aligned with STAR v2.6.1d[91] against the MesAur1.0 genome (GCA_000349665.1) and gene expression quantified using Salmon v1.5.2[92] in mapping-based mode. Secondary analysis was performed with SARTools v1.7. 4.[93] Samples from 2 to 4

independent hamsters per group were analyzed. Counts were normalized using the trimmed mean of M values method, and differential expression analysis was done with EdgeR v3.34.1.[93] P-values were adjusted by the Benjamini-Hochberg procedure, with features filtered based on an adjusted P-value threshold of 0.05. Volcano plots were created using the tidyverse and ggrepel packages to depict the log of adjusted P-values against the log ratio of differential expression. Differentially expressed genes or gene lists of interest were input into the Database for Annotation, Visualization, and Integrated Discovery (DAVID) for enrichment analysis related to Biological Processes and KEGG pathways.

Genomic DNA extraction and shotgun sequencing

Cecal samples were collected from young and aged non-infected (sacrificed 7 days after DMEM inoculation, termed D0) and SARS-CoV-2-infected (D7 and D22) hamsters. Cecum homogenates were stored at −80°C until analysis. Microbial DNA was extracted from approximately 150 mg of cecal samples (ZymoBIOMICS DNA Microprep Kit, Ozyme). Genomic DNA was purified with Agencourt AMPure XP magnetic beads (Beckman Coulter, Brea, CA) and quantified. Libraries were prepared from 17.5 ng of genomic DNA (DNA fragment and library prep kit, sparQ, QuantaBio, Beverly, MA, USA). Libraries pooled equimolarly at 2 nM concentration. Shotgun sequencing was performed using a 150-bp paired-end sequencing protocol on an NovaSeq 6000 platform (Illumina).

Metagenomic analysis

Raw metagenomics sequencing data were quality controlled using FastQC and MultiQC.[94] KneadData[95] was employed to remove human and host reads (*Homo sapiens*, GCF_000001405.40 and *Mesocricetus auratus*, GCF_017639785.1), adapters, and overrepresented sequences. Taxonomic classification was performed with Kraken 2, a system based on exact k-mer matches that inform a classification algorithm[96,97] using the database provided in the integrated Mouse Gut Metagenomic Catalog (iMGMC)[98] as reference, with the parameter – minimum-hit-groups set to 2 and the others kept as default. Then, abundances were estimated at the species level with Bracken (Bayesian Reestimation of Abundance with KrakEN), setting the read length parameter to 150. Taxonomy results were analyzed and visualized with R libraries phyloseq[99] and microViz (https://doi.org/10.21105/joss.03201). Taxonomy barplots were generated with the comp_barplot() function in microViz. Alpha-diversity (genus) was calculated with the ps_calc_diversity() function, using the Shannon index as measure. Beta-diversity (species) Aitchison metric was calculated with dist_calc(), Principal Coordinate Analysis visualization was obtained with ord_calc(), and Permanova statistics was calculated with multilevel pairwise comparison using pairwiseAdonis. Statistical analysis of differential abundant taxa was conducted with Microbiome Multivariable Association with Linear Models (Maaslin2),[57] with the parameters transform = "NONE", analysis_method = "CPLM", min_abundance = 0.01, max_significance = 0.05, and the others set as default. The HMP Unified Metabolic Analysis Network (HUMAnN) 3.0 software[56] was employed to evaluate the abundance and functional potential of the microbial communities. HUMAnN utilized the taxonomic profile generated by Kraken 2 and Bracken, and employed the ChocoPhlAn and UniRef databases for nucleotide and protein sequences mapping, respectively. KOs (KEGG Orthology) abundances obtained from HUMAnN 3.0 were uploaded to the gut-specific metabolic pathway analysis tool, GOmixer v1.7.5.0 (Raes Lab, Ghent, Belgium), for quantification of gut metabolic pathway modules. GOmixer employed a scaling method of multiplication by a scaling factor, utilized the median as the abundance estimator, and performed an automatic guess for the minimum module coverage cutoff. Statistical comparison of the identified gut metabolic pathway modules between groups was performed using MaAsLin2. The analysis employed a log transformation (transform = "LOG"), linear model (analysis_method = "LM"), and a significance threshold of α = 0.05. Default settings were used for all other parameters.

Metabolomic analysis

Hamster plasma samples were analyzed using a targeted quantitative approach based on the

MxP® Quant 500 kit (Biocrates Life Sciences AG, Innsbruck, Austria) using Flow Injection Analysis (FIA) and LC-MS/MS ($n = 3$–6/group).[37] The data filter excluded metabolites with more than 60% of missing values. For two metabolites, ornithine, and taurine, the missing values for some samples (aged mock number 4 for ornithine and samples from young mock number 2, aged mock number 5, and aged D7 number 1 for taurine) were replaced by the mean values of their respective group. Regarding data processing, the concentration (µM) raw data was normalized by sum, log-transformed and auto-scaled (mean-centered and divided by the standard deviation) and statistical analysis were performed by MetaboAnalyst 5.0.[100] Several analytical approaches were used to compare the experimental groups: Principal Component Analysis (PCA) was conducted using Euclidean distance. Hierarchical Clustering was performed using average linkage with Euclidean distance as the similarity metric. The resulting clusters were visualized in a heatmap, which displayed the top metabolites selected based on the lowest raw P-value from statistical tests (one-way ANOVA for multiple groups or T-test for two groups comparison). Random Forest Classification was employed to rank features by their contribution to classification accuracy, as measured by Mean Decrease Accuracy. For examining individual differences, Univariate analysis, showcasing fold changes with volcano plots specifically for non-infected young and aged hamsters was utilized. Two-way ANOVA, followed by Tukey's HSD post hoc test for further validation was used to assess the influence of age and infection on the plasma metabolome.

Correlations network analysis

For correlation analysis, metabolomics data was pre-processed by filtering the 53 modulated metabolites identified by random forest (Supplementary Table 3). This list identifies the features that most significantly influence the model's performance, thus facilitating the prioritization of metabolites for subsequent analyses. For metagenomics data, species-level relative abundance values were used for all groups. For early infection (D7 vs. D0) correlation analysis, we selected infection parameters including body weight, pneumonia score,

viral load, and lung gene expression as determined by quantitative RT-PCR. For the sake of simplicity, representative genes were chosen including *Cxcl10* (ISG), *Ccl2* (inflammation), and *Zo1* (barrier integrity). Late infection analysis (D22 vs. D0) additionally incorporated fibrosis score and expression of representative genes associated with fibrosis including *Col1a1*, *Col3a1*, *Mmp2*, and *Ecm1*. Hierarchical All-against-All association (HAllA)[101] was employed with the following parameters: Spearman's rank correlation coefficient as the similarity metric, Benjamini-Hochberg method for controlling the false discovery rate (FDR) at $\alpha = 0.05$, and default expected false negative rate (FNR) of 0.2 for detecting densely associated blocks. The significant associations were then integrated into a single table and imported into Cytoscape[102] for network visualization and analysis.

Statistical analyses

Except for the transcriptomics, metagenomics and metabolomics analyses, all statistical analyses were performed using GraphPad Prism v9.2.0 software. Due to the low number of replicates, the normality of the data could not be tested. A two tailed Mann-Whitney *U* test was used to compare two groups. Comparisons of more than two groups with each other were analyzed with the one-way ANOVA Kruskal-Wallis test (non-parametric), followed by Dunn's post-hoc test. Except for the transcriptomic analysis, data are expressed as the mean ± Standard Error of the Mean (MEM) or Standard Deviation (SD).

Disclosure statement

No potential conflict of interest was reported by the author(s).

Funding

ORCID

Vinícius de Rezende Rodovalho ⬚ http://orcid.org/0000-0003-4216-7143
Harry Sokol ⬚ http://orcid.org/0000-0002-2914-1822
François Trottein ⬚ http://orcid.org/0000-0003-3373-1814

Author contributions

FT and MARV conceived and supervised the study. FT designed the experiment. VS and FSA performed animal experiments. PBR, AD, JH, JFG and IW supervised the metabolomics analysis, and VRR, NB, HS, and MRV, supervised the gut microbiota composition analysis. DH performed the RNAseq analysis. PBR, VRR, NB, MARV and FT analyzed the data. LD and CR performed the IHC. PBR, VRR, LD, MRV and FT designed the figures. PBR, VRR, MARV and FT: drafted the manuscript. All authors revised the manuscript and provided critical comments. FT obtained funding.

Data availability statement

The sequence datasets (metagenomics) generated in this study are publicly available at https://www.ncbi.nlm.nih.gov/bioproject/PRJNA1121382(https://dataview.ncbi.nlm.nih.gov/object/PRJNA1121382?reviewer=gur7ir3sv1c33coljpo6df56rq). The sequence datasets (transcriptomics) generated in this study are publicly available at https://www.ncbi.nlm.nih.gov/bioproject/1118246. Metabolomics data are deposited to https://doi.org/10.57745/VHGKA8.

References

1. Bartleson JM, Radenkovic D, Covarrubias AJ, Furman D, Winer DA, Verdin E. SARS-CoV-2, COVID-19 and the ageing immune system. Nat Aging. 2021;1(9):769–782. doi: 10.1038/s43587-021-00114-7.
2. Rea IM, Alexander HD. Triple jeopardy in ageing: COVID-19, co-morbidities and inflamm-ageing. Ageing Res Rev. 2022;73:101494. doi: 10.1016/j.arr.2021.101494.
3. O'Driscoll M, Ribeiro Dos Santos G, Wang L, Cummings DAT, Azman AS, Paireau J, Fontanet A, Cauchemez S, Salje H. Age-specific mortality and immunity patterns of SARS-CoV-2. Nature. 2021;590(7844):140–145. doi: 10.1038/s41586-020-2918-0.
4. Schneider JL, Rowe JH, Garcia-de-Alba C, Kim CF, Sharpe AH, Haigis MC. The aging lung: physiology, disease, and immunity. Cell. 2021;184:1990–2019.
5. Boe DM, Boule LA, Kovacs EJ. Innate immune responses in the ageing lung. Clin Exp Immunol. 2017;187(1):16–25. doi: 10.1016/j.cell.2021.03.005.
6. Weckerle J, Mayr CH, Fundel-Clemens K, Lämmle B, Boryn L, Thomas MJ, Bretschneider T, Luippold AH, Huber HJ, Viollet C, et al. Transcriptomic and proteomic changes driving pulmonary fibrosis resolution in young and old mice. Am J Respir Cell Mol Biol. 2023;69(4):422–440. doi: 10.1165/rcmb.2023-0012OC.
7. McAleer JP, Kolls JK. Contributions of the intestinal microbiome in lung immunity. Eur J Immunol. 2018;48(1):39–49. doi: 10.1002/eji.201646721.
8. Sencio V, Machado MG, Trottein F. The lung–gut axis during viral respiratory infections: the impact of gut dysbiosis on secondary disease outcomes. Mucosal Immunol. 2021;14(2):296–304. doi: 10.1038/s41385-020-00361-8.
9. Zuo T, Zhang F, Lui GCY, Yeoh YK, Li AYL, Zhan H, Wan Y, Chung ACK, Cheung CP, Chen N, et al. Alterations in gut microbiota of patients with COVID-19 during time of hospitalization. Gastroenterology. 2020;159(3):944–955.e8. doi: 10.1053/j.gastro.2020.05.048.
10. Yeoh YK, Zuo T, Lui G-Y, Zhang F, Liu Q, Li AY, Chung AC, Cheung CP, Tso EY, Fung KS, et al. Gut microbiota composition reflects disease severity and dysfunctional immune responses in patients with COVID-19. Gut. 2021;70(4):698–706. doi: 10.1136/gutjnl-2020-323020.
11. Reinold J, Farahpour F, Fehring C, Dolff S, Konik M, Korth J, van Baal L, Hoffmann D, Buer J, Witzke O, et al. A pro-inflammatory gut microbiome characterizes SARS-CoV-2 infected patients and a reduction in the connectivity of an anti-inflammatory bacterial network associates with severe COVID-19. Front Cell Infect Microbiol. 2021;11:747816. doi: 10.3389/fcimb.2021.747816.
12. Schult D, Reitmeier S, Koyumdzhieva P, Lahmer T, Middelhoff M, Erber J, Schneider J, Kager J, Frolova M, Horstmann J, et al. Gut bacterial dysbiosis and instability is associated with the onset of complications and mortality in COVID-19. Gut Microbes.

2022;14(1):2031840. doi: 10.1080/19490976.2022. 2031840.

13. Sun Z, Song Z-G, Liu C, Tan S, Lin S, Zhu J, Dai F-H, Gao J, She J-L, Mei Z, et al. Gut microbiome alterations and gut barrier dysfunction are associated with host immune homeostasis in COVID-19 patients. BMC Med. 2022;20(1):24. doi: 10.1186/s12916-021-02212-0.

14. Gu S, Chen Y, Wu Z, Chen Y, Gao H, Lv L, Guo F, Zhang X, Luo R, Huang C, et al. Alterations of the gut microbiota in patients with coronavirus disease 2019 or H1N1 influenza. Clin Infect Dis Off Publ Infect Dis Soc Am. 2020;71:2669–2678. doi: 10.1093/cid/ciaa709.

15. Fuentes S, den Hartog G, Nanlohy NM, Wijnands L, Ferreira JA, Nicolaie MA, Pennings JLA, Jacobi R, de Wit J, van Beek J, et al. Associations of faecal microbiota with influenza-like illness in participants aged 60 years or older: an observational study. Lancet Healthy Longev. 2021;2(1):e13–23. doi: 10.1016/S2666-7568(20) 30034-9.

16. Zhang F, Wan Y, Zuo T, Yeoh YK, Liu Q, Zhang L, Zhan H, Lu W, Xu W, Lui GCY, et al. Prolonged impairment of short-chain fatty acid and L-Isoleucine biosynthesis in gut microbiome in patients with COVID-19. Gastroenterology. 2022;162(2):548–561. e4. doi: 10.1053/j.gastro.2021.10.013.

17. Chen Y, Gu S, Chen Y, Lu H, Shi D, Guo J, Wu W-R, Yang Y, Li Y, Xu K-J, et al. Six-month follow-up of gut microbiota richness in patients with COVID-19. Gut. 2022;71(1):222–225. doi: 10.1136/gutjnl-2021-324090.

18. Vestad B, Ueland T, Lerum TV, Dahl TB, Holm K, Barratt-Due A, Kåsine T, Dyrhol-Riise AM, Stiksrud B, Tonby K, et al. Respiratory dysfunction three months after severe COVID-19 is associated with gut microbiota alterations. J Intern Med. 2022;291(6):801–812. doi: 10.1111/joim.13458.

19. Essex M, Millet Pascual-Leone B, Löber U, Kuhring M, Zhang B, Brüning U, Fritsche-Guenther R, Krzanowski M, Fiocca Vernengo F, Brumhard S, et al. Gut microbiota dysbiosis is associated with altered tryptophan metabolism and dysregulated inflammatory response in COVID-19. NPJ Biofilms Microbiomes. 2024;10(1):66. doi: 10.1038/s41522-024-00538-0.

20. MacCann R, Ghosh TS, Garcia Leon AA, Li J, Negi R, Gaillard C, Saini G, Tinago W, Feeney ER, Yousif O, et al. Associations between host microbiome and inflammation suggest role for host microbiome in driving COVID-19 disease severity. Microbes Infect. 2024;26(3):105247. doi: 10.1016/j.micinf.2023.105247.

21. Li J, Ghosh TS, McCann R, Mallon P, Hill C, Draper L, Schult D, Fanning LJ, Shannon R, Sadlier C, et al. Robust cross-cohort gut microbiome associations with COVID-19 severity. Gut Microbes. 2023;15 (1):2242615. doi: 10.1080/19490976.2023.2242615.

22. Zhang F, Lau RI, Liu Q, Su Q, Chan FKL, Ng SC. Gut microbiota in COVID-19: key microbial changes, potential mechanisms and clinical applications. Nat

Rev Gastroenterol Hepatol. 2023;20(5):323–337. doi: 10.1038/s41575-022-00698-4.

23. Albrich WC, Ghosh TS, Ahearn-Ford S, Mikaeloff F, Lunjani N, Forde B, Suh N, Kleger G-R, Pietsch U, Frischknecht M, et al. A high-risk gut microbiota con-figuration associates with fatal hyperinflammatory immune and metabolic responses to SARS-CoV-2. Gut Microbes. 2022;14:2073131. doi: 10.1080/ 19490976.2022.2073131.

24. Liu Q, Mak JWY, Su Q, Yeoh YK, Lui G-Y, Ng SSS, Zhang F, Li AYL, Lu W, Hui D-C, et al. Gut microbiota dynamics in a prospective cohort of patients with post-acute COVID-19 syndrome. Gut. 2022;71 (3):544–552. doi: 10.1136/gutjnl-2021-325989.

25. Nouailles G, Wyler E, Pennitz P, Postmus D, Vladimirova D, Kazmierski J, Pott F, Dietert K, Muelleder M, Farztdinov V, et al. Temporal omics analysis in Syrian hamsters unravel cellular effector responses to moderate COVID-19. Nat Commun. 2021;12(1):4869. doi: 10.1038/s41467-021-25030-7.

26. Sencio V, Machelart A, Robil C, Benech N, Hoffmann E, Galbert C, Deryuter L, Heumel S, Hantute-Ghesquier A, Flourens A, et al. Alteration of the gut microbiota following SARS-CoV-2 infection correlates with disease severity in hamsters. Gut Microbes. 2022;14(1):2018900. doi: 10.1080/19490976. 2021.2018900.

27. Thevaranjan N, Puchta A, Schulz C, Naidoo A, Szamosi JC, Verschoor CP, Loukov D, Schenck LP, Jury J, Foley KP, et al. Age-associated microbial dysbio-sis promotes intestinal permeability, systemic inflam-mation, and macrophage dysfunction. Cell Host Microbe. 2018;23(4):570. doi: 10.1016/j.chom.2018.03. 006.

28. Ghosh TS, Shanahan F, O'Toole PW. The gut micro-biome as a modulator of healthy ageing. Nat Rev Gastroenterol Hepatol. 2022;19:565–584. doi: 10.1038/ s41575-022-00605-x.

29. Salazar N, Arboleya S, Fernández-Navarro T, de Los Reyes-Gavilán CG, Gonzalez S, Gueimonde M. Age-associated changes in gut microbiota and dietary com-ponents related with the immune system in adulthood and old age: a cross-sectional study. Nutrients. 2019;11 (8):1765. doi: 10.3390/nu11081765.

30. D'Amato A, Di Cesare Mannelli L, Lucarini E, Man AL, Le Gall G, Branca JJV, Ghelardini C, Amedei A, Bertelli E, Regoli M, et al. Faecal microbiota transplant from aged donor mice affects spatial learning and memory via modulating hippocampal synaptic plasticity- and neurotransmission-related proteins in young recipients. Microbiome. 2020;8(1):140. doi: 10. 1186/s40168-020-00914-w.

31. Lee J, Venna VR, Durgan DJ, Shi H, Hudobenko J, Putluri N, Petrosino J, McCullough G, Bryan RM. Young versus aged microbiota transplants to germ-free mice: increased short-chain fatty acids and improved cognitive performance. Gut Microbes.

2020;12(1):1814107–1814114. doi: 10.1080/19490976. 2020.1814107.

32. Ruiz-Ruiz S, Sanchez-Carrillo S, Ciordia S, Mena MC, Méndez-García C, Rojo D, Bargiela R, Zubeldia-Varela E, Martínez-Martínez M, Barbas C, et al. Functional microbiome deficits associated with ageing: chronological age threshold. Aging Cell. 2020;19(1):e13063. doi: 10.1111/acel.13063.

33. Lee J, d'Aigle J, Atadja L, Quaicoe V, Honarpisheh P, Ganesh BP, Hassan A, Graf J, Petrosino J, Putluri N, et al. Gut microbiota-derived short-chain fatty acids promote poststroke recovery in aged mice. Circ Res. 2020;127:453–465. doi: 10.1161/CIRCRESAHA.119. 316448.

34. Nagai M, Moriyama M, Ishii C, Mori H, Watanabe H, Nakahara T, Yamada T, Ishikawa D, Ishikawa T, Hirayama A, et al. High body temperature increases gut microbiota-dependent host resistance to influenza a virus and SARS-CoV-2 infection. Nat Commun. 2023;14(1):3863. doi: 10.1038/s41467-023-39569-0.

35. Antunes KH, Fachi JL, de Paula R, da Silva EF, Pral LP, Dos Santos AÁ, Dias GBM, Vargas JE, Puga R, Mayer FQ, et al. Microbiota-derived acetate protects against respiratory syncytial virus infection through a GPR43-type 1 interferon response. Nat Commun. 2019;10(1):3273. doi: 10.1038/s41467-019-11152-6.

36. Trompette A, Gollwitzer ES, Pattaroni C, Lopez-Mejia IC, Riva E, Pernot J, Ubags N, Fajas L, Nicod LP, Marsland BJ. Dietary fiber confers protection against flu by shaping Ly6c– patrolling monocyte hematopoiesis and CD8+ T cell metabolism. Immunity. 2018;48 (5):992–1005.e8. doi: 10.1016/j.immuni.2018.04.022.

37. Heumel S, de Rezende Rodovalho V, Urien C, Specque F, Brito Rodrigues P, Robil C, Delval L, Sencio V, Descat A, Deruyter L, et al. Shotgun metagenomics and systemic targeted metabolomics highlight indole-3-propionic acid as a protective gut microbial metabolite against influenza infection. Gut Microbes. 2024;16(1):2325067. doi: 10.1080/19490976.2024. 2325067.

38. Haak BW, Littmann ER, Chaubard J-L, Pickard AJ, Fontana E, Adhi F, Gyaltshen Y, Ling L, Morjaria SM, Peled JU, et al. Impact of gut colonization with butyrate-producing microbiota on respiratory viral infection following allo-hct. Blood. 2018;131:2978–2986. doi: 10.1182/blood-2018-01-828996.

39. Sencio V, Machado MG, Trottein F. The lung–gut axis during viral respiratory infections: the impact of gut dysbiosis on secondary disease outcomes. Mucosal Immunol. 2021;14:296–304. doi: 10.1038/s41385-020-00361-8.

40. Seibert B, Cáceres CJ, Carnaccini S, Cardenas-Garcia S, Gay LC, Ortiz L, Geiger G, Rajao DS, Ottesen E, Perez DR, et al. Pathobiology and dysbiosis of the respiratory and intestinal microbiota in 14 months old Golden Syrian hamsters infected with SARS-CoV-2.

PLOS Pathog. 2022;18(10):e1010734. doi: 10.1371/journal.ppat.1010734.

41. DeJong EN, Surette MG, Bowdish DME. The gut microbiota and unhealthy aging: disentangling cause from consequence. Cell Host Microbe. 2020;28:180–189. doi: 10.1016/j.chom.2020.07.013.

42. Zhang X, Yang Y, Su J, Zheng X, Wang C, Chen S, Liu J, Lv Y, Fan S, Zhao A, et al. Age-related compositional changes and correlations of gut microbiome, serum metabolome, and immune factor in rats. GeroScience. 2021;43(2):709–725. doi: 10.1007/s11357-020-00188-y.

43. Wilmanski T, Diener C, Rappaport N, Patwardhan S, Wiedrick J, Lapidus J, Earls JC, Zimmer A, Glusman G, Robinson M, et al. Gut microbiome pattern reflects healthy ageing and predicts survival in humans. Nat Metab. 2021;3(2):274–286. doi: 10.1038/s42255-021-00348-0.

44. Sencio V, Benech N, Robil C, Deruyter L, Heumel S, Machelart A, Sulpice T, Lamazière A, Grangette C, Briand F, et al. Alteration of the gut microbiota's composition and metabolic output correlates with COVID-19-like severity in obese NASH hamsters. Gut Microbes. 2022;14(1):2100200. doi: 10.1080/19490976. 2022.2100200.

45. Zarei I, Koistinen VM, Kokla M, Klåvus A, Babu AF, Lehtonen M, Auriola S, Hanhineva K. Tissue-wide metabolomics reveals wide impact of gut microbiota on mice metabolite composition. Sci Rep. 2022;12:15018. doi: 10.1038/s41598-022-19327-w.

46. Tanaka H, Sirich TL, Meyer TW. Uremic solutes produced by colon microbes. Blood Purif. 2015;40 (4):306–311. doi: 10.1159/000441578.

47. Han J, Wang Z, Lu C, Zhou J, Li Y, Ming T, Zhang Z, Wang ZJ, Su X. The gut microbiota mediates the protective effects of anserine supplementation on hyperuricaemia and associated renal inflammation. Food Funct. 2021;12(19):9030–9042. doi: 10.1039/d1fo01884a.

48. Bárcena C, Valdés-Mas R, Mayoral P, Garabaya C, Durand S, Rodríguez F, Fernández-García MT, Salazar N, Nogacka AM, Garatachea N, et al. Healthspan and lifespan extension by fecal microbiota transplantation into progeroid mice. Nat Med. 2019;25 (8):1234–1242. doi: 10.1038/s41591-019-0504-5.

49. Kundu P, Lee HU, Garcia-Perez I, Tay EXY, Kim H, Faylon LE, Martin KA, Purbojati R, Drautz-Moses DI, Ghosh S, et al. Neurogenesis and prolongevity signaling in young germ-free mice transplanted with the gut microbiota of old mice. Sci Transl Med. 2019;11: eaau4760. doi: 10.1126/scitranslmed.aau4760.

50. Shin J, Noh J-R, Choe D, Lee N, Song Y, Cho S, Kang E-J, Go M-J, Ha SK, Chang D-H, et al. Ageing and rejuvenation models reveal changes in key microbial communities associated with healthy ageing. Microbiome. 2021;9:240. doi: 10.1186/s40168-021-01189-5.

51. Parker A, Romano S, Ansorge R, Aboelnour A, Le Gall G, Savva GM, Pontifex MG, Telatin A, Baker D, Jones E, et al. Fecal microbiota transfer between young and aged mice reverses hallmarks of the aging gut, eye, and brain. Microbiome. 2022;10(1):68. doi: 10.1186/s40168-022-01243-w.

52. Delval L, Hantute-Ghesquier A, Sencio V, Flaman JM, Robil C, Angulo FS, Lipskaia L, Çobanoğlu O, Lacoste A-S, Machelart A, et al. Removal of senescent cells reduces the viral load and attenuates pulmonary and systemic inflammation in SARS-CoV-2-infected, aged hamsters. Nat Aging. 2023;3:829–845. doi: 10.1038/s43587-023-00442-w.

53. Chen J, Wu J, Hao S, Yang M, Lu X, Chen X, Li L. Long term outcomes in survivors of epidemic influenza a (H7N9) virus infection. Sci Rep. 2017;7(1):17275. doi: 10.1038/s41598-017-17497-6.

54. Keeler SP, Agapov EV, Hinojosa ME, Letvin AN, Wu K, Holtzman MJ. Influenza a virus infection causes chronic lung disease linked to sites of active viral RNA remnants. J Immunol Baltim Md 1950. 2018;201:2354–2368. doi: 10.4049/jimmunol.1800671.

55. Goplen NP, Wu Y, Son YM, Li C, Wang Z, Cheon IS, Jiang L, Zhu B, Ayasoufi K, Chini EN, et al. Tissue-resident CD8+ T cells drive age-associated chronic lung sequelae after viral pneumonia. Sci Immunol. 2020;5 (53):eabc4557. doi: 10.1126/sciimmunol.abc4557.

56. Beghini F, McIver LJ, Blanco-Míguez A, Dubois L, Asnicar F, Maharjan S, Mailyan A, Manghi P, Scholz M, Thomas AM, et al. Integrating taxonomic, functional, and strain-level profiling of diverse microbial communities with bioBakery 3. eLife. 2021;10: e65088. doi: 10.7554/eLife.65088.

57. Mallick H, Rahnavard A, McIver LJ, Ma S, Zhang Y, Nguyen LH, Tickle TL, Weingart G, Ren B, Schwager EH, et al. Multivariable association discovery in population-scale meta-omics studies. PLOS Comput Biol. 2021;17:e1009442. doi: 10.1371/journal.pcbi.1009442.

58. Richard VR, Gaither C, Popp R, Chaplygina D, Brzhozovskiy A, Kononikhin A, Mohammed Y, Zahedi RP, Nikolaev EN, Borchers CH. Early prediction of COVID-19 patient survival by targeted plasma multi-omics and machine learning. Mol Cell Proteomics MCP. 2022;21(10):100277. doi: 10.1016/j.mcpro.2022.100277.

59. Abdallah AM, Doudin A, Sulaiman TO, Jamil O, Arif R, Sada FA, Yassine HM, Elrayess MA, Elzouki A-N, Emara MM, et al. Metabolic predictors of COVID-19 mortality and severity: a survival analysis. Front Immunol. 2024;15:1353903. doi: 10.3389/fimmu.2024.1353903.

60. Danlos F-X, Grajeda-Iglesias C, Durand S, Sauvat A, Roumier M, Cantin D, Colomba E, Rohmer J, Pommeret F, Baciarello G, et al. Metabolomic analyses of COVID-19 patients unravel stage-dependent and

61. Matsumoto M, Kibe R, Ooga T, Aiba Y, Kurihara S, Sawaki E, Koga Y, Benno Y. Impact of intestinal microbiota on intestinal luminal metabolome. Sci Rep. 2012;2 (1):233. doi: 10.1038/srep00233.

62. Galkin F, Mamoshina P, Aliper A, Putin E, Moskalev V, Gladyshev VN, Zhavoronkov A. Human gut microbiome aging clock based on taxonomic profiling and deep learning. iScience. 2020;23(6):101199. doi: 10.1016/j.isci.2020.101199.

63. Wu J, Ren W, Chen L, Lou Y, Liu C, Huang Y, Hu Y. Age-related changes in the composition of intestinal microbiota in elderly Chinese individuals. Gerontology. 2022;68:976–988. doi: 10.1159/000520054.

64. Cheng J, Laitila A, Ouwehand AC. Bifidobacterium animalis subsp. lactis HN019 effects on gut health: a review. Front Nutr. 2021;8:790561. doi: 10.3389/fnut.2021.790561.

65. Uusitupa H-M, Rasinkangas P, Lehtinen MJ, Mäkelä SM, Airaksinen K, Anglenius H, Ouwehand AC, Maukonen J. Bifidobacterium animalis subsp. lactis 420 for metabolic health: review of the research. Nutrients. 2020;12(4):892. doi: 10.3390/nu12040892.

66. Chuandong Z, Hu J, Li J, Wu Y, Wu C, Lai G, Shen H, Wu F, Tao C, Liu S, et al. Distribution and roles of Ligilactobacillus murinus in hosts. Microbiol Res. 2024;282:127648. doi: 10.1016/j.micres.2024.127648.

67. Luan Z, Sun G, Huang Y, Yang Y, Yang R, Li C, Wang T, Tan D, Qi S, Jun C, et al. Metagenomics study reveals changes in gut microbiota in Centenarians: a cohort study of Hainan centenarians. Front Microbiol. 2020;11:1474. doi: 10.3389/fmicb.2020.01474.

68. Abiri B, Vafa M. The role of nutrition in attenuating age-related skeletal muscle atrophy. Adv Exp Med Biol. 2020;1260:297–318. doi: 10.1007/978-3-030-42667-5_12.

69. Song R, Hu M, Qin X, Qiu L, Wang P, Zhang X, Liu R, Wang X. The roles of lipid metabolism in the pathogenesis of chronic diseases in the elderly. Nutrients. 2023;15(15):3433. doi: 10.3390/nu15153433.

70. Rokicki J, Li L, Imabayashi E, Kaneko J, Hisatsune T, Matsuda H. Daily carnosine and anserine supplementation alters verbal episodic memory and resting state network connectivity in healthy elderly adults. Front Aging Neurosci. 2015;7:219. doi: 10.3389/fnagi.2015.00219.

71. Kaneko J, Enya A, Enomoto K, Ding Q, Hisatsune T. Anserine (beta-alanyl-3-methyl-L-histidine) improves neurovascular-unit dysfunction and spatial memory in aged AβPPswe/PSEN1dE9 Alzheimer's-model mice. Sci Rep. 2017;7(1):12571. doi: 10.1038/s41598-017-12785-7.

72. Wypych TP, Pattaroni C, Perdijk O, Yap C, Trompette A, Anderson D, Creek DJ, Harris NL, Marsland BJ. Microbial metabolism of L-tyrosine

prognostic biomarkers. Cell Death Dis. 2021;12 (3):258. doi: 10.1038/s41419-021-03540-y.

protects against allergic airway inflammation. Nat Immunol. 2021;22(3):279–286. doi: 10.1038/s41590-020-00856-3.

73. Sencio V, Barthelemy A, Tavares LP, Machado MG, Soulard D, Cuinat C, Queiroz-Junior CM, Noordine M-L, Salomé-Desnoulez S, Deryuter L, et al. Gut dysbiosis during influenza contributes to pulmonary Pneumococcal superinfection through altered short-chain fatty acid production. Cell Rep. 2020;30:2934–2947.e6. doi: 10.1016/j.celrep.2020.02.013.

74. Mendes de Almeida V, Engel DF, Ricci MF, Cruz CS, Lopes ÍS, Alves DA, Auriol M, Magalhães J, Machado EC, Rocha VM, et al. Gut microbiota from patients with COVID-19 cause alterations in mice that resemble post-covid symptoms. Gut Microbes. 2023;15:2249146. doi: 10.1080/19490976.2023.2249146 .

75. Sencio V, Gallerand A, Gomes Machado M, Deruyter L, Heumel S, Soulard D, Barthelemy J, Cuinat C, Vieira AT, Barthelemy A, et al. Influenza virus infection impairs the gut's barrier properties and favors secondary enteric bacterial infection through reduced production of short-chain fatty acids. Infect Immun. 2021;89:e0073420. doi: 10.1128/IAI.00734-20.

76. Sokol H, Contreras V, Maisonnasse P, Desmons A, Delache B, Sencio V, Machelart A, Brisebarre A, Humbert L, Deryuter L, et al. SARS-CoV-2 infection in nonhuman primates alters the composition and functional activity of the gut microbiota. Gut Microbes. 2021;13(1):1–19. doi: 10.1080/19490976.2021.1893113.

77. Nabizadeh E, Memar MY, Hamishehkar H, Ghanbari H, Kadkhoda H, Asnaashari S, Kafil HS, Varshochi M, Mostafazadeh M, Hosseinpour R, et al. Short-chain fatty acids profile in patients with SARS-CoV-2: a case-control study. Health Sci Rep. 2023;6:e1411. doi: 10.1002/hsr2.1411.

78. Cross AJ, Major JM, Rothman N, Sinha R. Urinary 1-methylhistidine and 3-methylhistidine, meat intake, and colorectal adenoma risk. Eur J Cancer Prev. 2014;23 (5):385–390. doi: 10.1097/CEJ.0000000000000027.

79. Engelen MPKJ, Kirschner SK, Coyle KS, Argyelan D, Neal G, Dasarathy S, Deutz NEP. Sex related differences in muscle health and metabolism in chronic obstructive pulmonary disease. Clin Nutr Edinb Scotl. 2023;42:1737–1746. doi: 10.1016/j.clnu.2023.06.031.

80. Damanti S, Cristel G, Ramirez GA, Bozzolo EP, Da Prat V, Gobbi A, Centurioni C, Di Gaeta E, Del Prete A, Calabrò MG, et al. Influence of reduced muscle mass and quality on ventilator weaning and complications during intensive care unit stay in COVID-19 patients. Clin Nutr Edinb Scotl. 2022;41 (12):2965–2972. doi: 10.1016/j.clnu.2021.08.004.

81. Meyer H-J, Wienke A, Surov A. Computed tomography-defined body composition as prognostic markers for unfavourable outcomes and in-hospital mortality in coronavirus disease 2019. J Cachexia Sarcopenia Muscle. 2022;13(1):159–168. doi: 10.1002/jcsm.12868.

82. McGovern J, Dolan R, Richards C, Laird BJ, McMillan DC, Maguire D. Relation between body composition, systemic inflammatory response, and clinical outcomes in patients admitted to an urban teaching hospital with COVID-19. J Nutr. 2021;151 (8):2236–2244. doi: 10.1093/jn/nxab142.

83. Barberis E, Timo S, Amede E, Vanella VV, Puricelli C, Cappellano G, Raineri D, Cittone MG, Rizzi E, Pedrinelli AR, et al. Large-scale plasma analysis revealed new mechanisms and molecules associated with the host response to SARS-CoV-2. Int J Mol Sci. 2020;21(22):8623. doi: 10.3390/ijms21228623.

84. Maltais-Payette I, Lajeunesse-Trempe F, Pibarot P, Biertho L, Tchernof A. Association between circulating amino acids and COVID-19 severity. Metabolites. 2023;13:201. doi: 10.3390/ijms21228623.

85. Lawler NG, Gray N, Kimhofer T, Boughton B, Gay M, Yang R, Morillon A-C, Chin S-T, Ryan M, Begum S, et al. Systemic perturbations in Amine and kynurenine metabolism associated with acute SARS-CoV-2 infection and inflammatory cytokine responses. J Proteome Res. 2021;20(5):2796–2811. doi: 10.1021/acs.jproteome.1c00052.

86. Li M, Ding Y, Wei J, Dong Y, Wang J, Dai X, Yan J, Chu F, Zhang K, Meng F, et al. Gut microbiota metabolite indole-3-acetic acid maintains intestinal epithelial homeostasis through mucin sulfation. Gut Microbes. 2024;16(1):2377576. doi: 10.1080/19490976.2024.2377576.

87. Krishnan S, Ding Y, Saeidi N, Choi M, Sridharan GV, Sherr DH, Yarmush ML, Alaniz RC, Jayaraman A, Lee K. Gut microbiota-derived tryptophan metabolites modulate inflammatory response in hepatocytes and macrophages. Cell Rep. 2019;28(12):3285. doi: 10.1016/j.celrep.2019.08.080.

88. Shaheen N, Miao J, Li D, Xia B, Baoyinna B, Zhao Y, Zhao J. Indole-3-acetic acid protects against lipopolysaccharide-induced endothelial cell dysfunction and lung injury through the activation of USP40. Am J Respir Cell Mol Biol. 2024;71:307–317. doi: 10.1016/j.celrep.2018.03.109.

89. Albrich WC, Ghosh TS, Ahearn-Ford S, Mikaeloff F, Lunjani N, Forde B, Suh N, Kleger G-R, Pietsch U, Frischknecht M, et al. A high-risk gut microbiota configuration associates with fatal hyperinflammatory immune and metabolic responses to SARS-CoV-2. Gut Microbes. 2022;14(1):2073131. doi: 10.1080/19490976.2022.2073131.

90. Frere JJ, Serafini RA, Pryce KD, Zazhytska M, Oishi K, Golynker I, Panis M, Zimering J, Horiuchi S, Hoagland DA, et al. SARS-CoV-2 infection in hamsters and humans results in lasting and unique systemic perturbations after recovery. Sci Transl Med. 2022;14 (664):eabq3059. doi: 10.1126/scitranslmed.abq3059.

91. Dobin A, Davis CA, Schlesinger F, Drenkow J, Zaleski C, Jha S, Batut P, Chaisson M, Gingeras TR. STAR: ultrafast universal RNA-seq aligner. Bioinforma Oxf Engl. 2013;29 (1):15–21. doi: 10.1093/bioinformatics/bts635.

92. Patro R, Duggal G, Love MI, Irizarry RA, Kingsford C. Salmon provides fast and bias-aware quantification of transcript expression. Nat Methods. 2017;14 (4):417–419. doi: 10.1038/nmeth.4197.

93. Varet H, Brillet-Guéguen L, Coppée J-Y, Dillies M-A, Mills K. Sartools: a DESeq2- and EdgeR-based R pipeline for comprehensive differential analysis of RNA-Seq data. PLOS ONE. 2016;11(6):e0157022. doi: 10.1371/journal.pone.0157022.

94. Ewels P, Magnusson M, Lundin S, Käller M. MultiQC: summarize analysis results for multiple tools and samples in a single report. Bioinforma Oxf Engl. 2016;32 (19):3047–3048. doi: 10.1093/bioinformatics/btw354.

95. McIver LJ, Abu-Ali G, Franzosa EA, Schwager R, Morgan XC, Waldron L, Segata N, Huttenhower C. bioBakery: a meta'omic analysis environment. Bioinforma Oxf Engl. 2018;34:1235–1237. doi: 10.1093/bioinformatics/btx75.

96. Wood DE, Lu J, Langmead B. Improved metagenomic analysis with kraken 2. Genome Biol. 2019;20(1):257. doi: 10.1186/s13059-019-1891-0.

97. Lu J, Rincon N, Wood DE, Breitwieser FP, Pockrandt C, Langmead B, Salzberg SL, Steinegger M. Metagenome analysis using the Kraken software suite.

Nat Protoc. 2022;17:2815–2839. doi: 10.1038/s41596-022-00738-y.

98. Lesker TR, Durairaj AC, Gálvez EJC, Lagkouvardos I, Baines JF, Clavel T, Sczyrba A, McHardy AC, Strowig T. An integrated metagenome catalog reveals new insights into the murine gut microbiome. Cell Rep. 2020;30:2909–2922.e6. doi: 10.1016/j.celrep.2020.02.036.

99. McMurdie PJ, Holmes S, Watson M. Phyloseq: an R package for reproducible interactive analysis and graphics of microbiome census data. PLOS ONE. 2013;8(4):e61217. doi: 10.1371/journal.pone.0061217.

100. Xia J, Wishart DS. Web-based inference of biological patterns, functions and pathways from metabolomic data using MetaboAnalyst. Nat Protoc. 2011;6:743–760. doi: 10.1038/nprot.2011.319.

101. Ghazi AR, Sucipto K, Rahnavard A, Franzosa EA, McIver LJ, Lloyd-Price J, Schwager E, Weingart G, Moon YS, Morgan XC, et al. High-sensitivity pattern discovery in large, paired multiomic datasets. Bioinforma Oxf Engl. 2022;38(Supplement_1):i378–85. doi: 10.1093/bioinformatics/btac232.

102. Shannon P, Markiel A, Ozier O, Baliga NS, Wang JT, Ramage D, Amin N, Schwikowski B, Ideker T. Cytoscape: a software environment for integrated models of biomolecular interaction networks. Genome Res. 2003;13(11):2498–2504. doi: 10.1101/gr.1239303.